Lab on a Chip

CRITICAL REVIEW

View Article Online
View Journal | View Issue

Cite this: *Lab Chip*, 2026, **26**, 1299

Twenty years of microfluidic probes and open-space microfluidics: from origins to emerging directions

Dima Samer Ali,[ab] Ayoub Glia[ac] and Mohammad A. Qasaimeh *[abcde]

Microfluidic probes (MFPs) are an emerging class of open microfluidic devices that use hydrodynamic flow confinement (HFC) to enable precise, contact-free delivery, and removal of fluids on biological surfaces. Unlike closed-channel microfluidics, MFPs operate in open environments, allowing localized chemical and biological interactions with high spatial and temporal resolution. Since their introduction in 2005, MFPs have advanced through major innovations, including multipolar flow designs, vertical configurations, 3D printing, and structural enhancements such as herringbone micromixers. This review presents a comprehensive overview of MFP technologies, covering core physical principles, flow dynamics, operating modes, and the influence of geometric and hydrodynamic design. We examine fabrication techniques such as photolithography, soft lithography, and 3D printing, highlighting their trade-offs in precision, scalability, and cost. We also explore biological applications of MFPs, including tissue assays, cellular manipulation, molecular patterning, and single-cell biopsy. Emerging integrations with heating, dielectrophoresis, and real-time feedback are expanding the utility of MFPs for adaptive high-throughput workflows. By tracing two decades of development, this review positions MFPs as transformative tools in open-space microfluidics and outlines opportunities for future progress.

Received 14th September 2025,
Accepted 15th January 2026

DOI: 10.1039/d5lc00879d

rsc.li/loc

1 Introduction

The field of microfluidics involves the precise control and manipulation of microscale volumes of liquid, typically within engineered miniaturized channels, ranging from 10 to 1000 μm in dimensions.[1] These systems offer numerous advantages for chemical and biological analysis, including high resolution and sensitivity, minimal sample and reagent consumption, rapid processing, and compact device footprints.[2] Microfluidics has expanded through advances in molecular biology, microelectronics, and point-of-care diagnostics. It has enabled the development of "lab-on-a-chip" systems capable of performing a wide range of functions, from high-throughput screening[3] and protein crystallization[4,5] to cell manipulation[6] and single-molecule[7] studies. Several practical microanalytical systems[8–11] were also established. Despite its transformative potential, early microfluidic systems relied predominantly on closed-channel configurations, which posed limitations on sample size and made interfacing with the macroscopic environment difficult. These challenges became especially evident when transporting reagents to large substrates such as slides, Petri dishes, or tissue sections, which proved impractical using traditional chip-based microchannels. To address this, new strategies were required to "open" microfluidics beyond the confines of enclosed physical channels. One of the earliest contributions to this field was reported in 2004. Named open air microfluidics, the microfluidic streams were integrated with micropipette-based single-cell manipulation and were open to air (with no roof).[12] This study demonstrated how open-channel configurations enable functionalities such as intracellular injection and patch-clamp recording, highlighting the versatility and early potential of open microfluidics.

The microfluidic probe (MFP) emerged as another branch that adopts the open microfluidics concepts. Developed in 2005 by Juncker *et al.*,[13] the MFP combined microfluidics with the concept of a scanning probe, creating a mobile, microscale flow tool that operates in open space. In the MFP design, microscopic apertures for liquid injection and aspiration are positioned in proximity, typically within tens of micrometers, above a target surface. By controlling the ratio of aspiration to injection flow rates above a specific threshold, a hydrodynamically confined liquid stream forms

[a] *Engineering Division, New York University Abu Dhabi, United Arab Emirates. E-mail: maq4@nyu.edu*
[b] *Mechanical and Aerospace Engineering, New York University, NY 10012, USA*
[c] *Research Center for Translational Medical Devices (CENTMED), New York University Abu Dhabi, Abu Dhabi, United Arab Emirates*
[d] *Department of Biomedical Engineering, Tandon School of Engineering, New York University, New York City, NY, USA*
[e] *NYU-KAIST Global Innovation and Research Institute, New York, USA*

between the probe's tip and the substrate. This replaces the solid walls of conventional channels with dynamically shaped fluid boundaries. Repositioning the probe relative to the substrate allows the confined stream to scan across the surface, enabling targeted delivery and removal of reagents. This capability overcame key limitations of solid-walled microchannels, since fluid boundaries could now be generated and controlled in real time. The MFP is mobile and can process large samples *in situ*, something that could not be achieved using monolithic microfluidic chips. Early demonstrations highlighted the versatility of the MFP. The device was used to pattern biomolecules, generate steep chemical gradients on open surfaces, perform localized staining, and detach individual cells in a controlled manner. These experiments illustrated how miniaturized, wall-less flow confinement can interact with specific regions of a surface without disturbing adjacent areas. They further showed that MFPs overcome many of the limitations associated with closed-channel systems.[13] By enabling localized microfluidic operations on large, accessible samples such as tissues or slides, the MFP helped redefine the scope of open microfluidic applications in bioscience.

Building on the success of the classical two-port MFP, which is the basic hydrodynamic configuration consisting of one injection and one aspiration aperture forming a confined teardrop-shaped flow region (traditionally known as the dipole configuration), researchers sought to expand the technology's capabilities by exploring multipolar flow configurations, which denotes higher-order arrangements generated by multiple injection/aspiration pairs. While the original MFP operated as a simple flow dipole, the idea emerged that multiple injection and aspiration points could enable more complex flow patterns. This was demonstrated in 2011 by Qasaimeh *et al.* with the introduction of the microfluidic quadrupole (MQ).[14] In this system, two pairs of opposing apertures were used to simultaneously inject and aspirate fluids, creating a four-point flow arrangement. The intersecting flows formed a central stagnation zone where convection was canceled out, similar to the null point in an electrostatic quadrupole. By introducing a reagent through one of the apertures, the researchers established a stationary and tunable concentration gradient within the open fluid volume. This "floating" gradient could be repositioned in real time by adjusting flow rates, offering a new level of control not achievable with basic two-port probes. The MQ represented a significant step forward in open microfluidics, stable gradient generation and localized stimulation in dynamic environments. This shift from dipolar to multipolar flow confinement allowed researchers to replicate more intricate biochemical landscapes, such as chemical gradients or localized mixing zones, with fine spatial and temporal precision. In parallel with these conceptual advances, the vertical microfluidic probe (vMFP) was introduced as a practical redesign.[15] In the vMFP, the probe head is oriented vertically above the sample, which simplifies alignment, reduces fluid leakage, and improves scanning precision. Introduced by Kaigala *et al.* in 2011,[15] the vMFP addressed several challenges of the original design and helped improve MFP reliability. This vertical format supported broader use cases, from nanoscale patterning to delicate cell processing, while preserving the advantages of operating in open space.

A major engineering milestone in the development of MFPs was the adoption of additive manufacturing techniques. Brimmo *et al.* were the first to demonstrate the use of high-resolution 3D printing to fabricate an integrated MFP head, offering both scalability and design flexibility.[16] This approach eliminated the reliance on cleanroom-based fabrication, enabling rapid prototyping of intricate geometries such as curved or multilayered channels. The 3D-printed MFP maintained precise hydrodynamic flow confinement and was validated in biologically relevant assays, including subcellular delivery and multiplexed biochemical stimulation. This achievement was not only a technical advance but also a testament to the value of interdisciplinary collaboration. It resulted from a joint effort between engineering and biological research groups, bringing together design innovation and biomedical insight. The use of 3D printing marked a pivotal shift, making MFP technology more accessible and adaptable, and laying the groundwork for future advances in diagnostics, screening, and therapeutic development.

The impact of this advancement helped solidify the MFP as a central tool in the expanding field of open microfluidics. Unlike closed microchannels that confine flow within permanent walls, open systems allow greater flexibility in how fluids interact with samples and instrumentation. In the case of the MFP, the open configuration permits unobstructed access to the area of fluid exposure, enabling real-time observation and precise intervention at targeted locations.[17] This is particularly advantageous for biological applications. The MFP can deliver stimuli to a selected single cell or extract analytes from a small, localized region on an open culture dish, which would be exceedingly difficult to achieve with closed-chip devices.[17] Moreover, open formats like the MFP simplify integration with other analytical techniques such as microscopy and chemical sensing, since there are no channel walls blocking optical or physical access to the reaction zone. These advantages help explain why the MFP approach, although conceptually distinct from classical microfluidic chips, has become so influential. It unites the precision of microfluidics with the mobility of scanning probes and the accessibility of macroscale experimentation. This enables the formation of finely localized concentration fields and controlled reagent interfaces at microscale resolution on surfaces of interest, while still operating in an open environment. This capability has contributed to the emergence of open-space microfluidics as a distinct subfield within the broader microfluidics landscape.[18]

In the following sections, we present a comprehensive overview of microfluidic probes, beginning with their definition and significance as foundational tools in open microfluidics. We examine the key principles underlying their

operation, including hydrodynamic configurations and flow confinement mechanisms. Fabrication strategies such as photolithography and 3D printing are reviewed in detail, along with the materials used across different MFP architectures. We then discuss advanced functional integrations, including electrical and thermal coupling, that have expanded the technological capabilities of MFPs. This is followed by an overview of their biological and analytical applications, such as localized tissue processing, single-cell manipulation, subcellular stimulation, and molecular bio-patterning. Finally, we highlight current limitations and outline promising directions for future development. Through this structure, the review aims to trace the evolution of MFPs, emphasize their growing impact across disciplines, and offer a forward-looking perspective on opportunities ahead. In contrast to earlier reviews,[19,20] the present work offers the first comprehensive synthesis of microfluidic probe development from the inaugural publication through 2025. Moreover, this review also serves as a conceptual and practical tutorial, integrating theory, operational parameters, fabrication and integration strategies, and applications to provide a unified framework for researchers entering or advancing in the field.

2 Concepts and configurations

MFPs enable precise, contact-free fluid manipulation by combining specific structural features with principles of hydrodynamic flow confinement (HFC), in which fluid streams are shaped and confined through the balance of injection and aspiration. This allows localized chemical processing on open surfaces with high spatial resolution. MFP performance depends on geometric parameters such as aperture size, spacing, and the mesa-to-substrate gap, as well as flow parameters including injection and aspiration rates. Beyond basic dipolar designs, advanced configurations such as multipoles, hierarchical confinements, and pixelated arrays have significantly extended the functional range of MFPs. These innovations have reinforced their value as versatile platforms across biomedical and analytical applications.

2.1 The MFP device

Closed microfluidic devices typically involve introducing, processing, or culturing cells within sealed compartments. While microchannels offer precise control over fluid transport, they present several limitations. Shear forces from fluid flow can exert mechanical stress on cells, leading to membrane damage or altered behavior. The small dimensions of closed systems can restrict the diffusion of nutrients and oxygen, especially in dense cultures, and may promote the accumulation of metabolic waste, resulting in local toxicity. Physical confinement also limits cell expansion and tissue organization, making it difficult to replicate physiologically relevant structures. Most critically, retrieving cells from enclosed systems can be challenging, which may affect cell viability and complicate downstream analyses such as gene or protein expression studies.[13]

The open microfluidic design of the MFP merges the benefits of hydrodynamic flow confinement with the mobility of scanning probes.[13] A defining feature of the MFP is its exceptional spatiotemporal flexibility for manipulating and chemically stimulating samples with precision.[18] In the review by Kaigala *et al.*, the open-space framework for performing localized chemistry was thoroughly presented, highlighting three technologies including the HFC principle. The review presented how HFC enables micrometer-scale control of chemical and biological confinements through localized reagent delivery to surfaces and cells without physical barriers.[19]

In its most basic form, the body of an MFP consists of three main components: the mesa, which contains the injection and aspiration apertures; the internal channels and fluidic ports; and the holder lock mechanism, as shown in Fig. 1. The flat tip at the bottom of the MFP, known as the mesa, incorporates at least one pair of apertures connected to the device connection ports through internal channels. These ports accommodate compatible fittings for tubing, allowing the MFP to be connected to a pressure-driven flow system for injecting and aspirating fluids. The injected fluid, referred to as the processing fluid, passes through the injection apertures toward the substrate. This fluid may consist of a buffer dosed with pharmacological agents, a solution spiked with proteins or DNA, or a biological sample such as blood or a cell suspension. The aspirated fluids include the processing fluid after surface interaction, the immersion fluid, and any dissociated biological components such as proteins, cells, or other analytes.

Finally, the MFP can be clamped at the edges with an aluminum manipulator rod,[13] mounted on a custom-built holder that couples to the tubing connected to external pumps.[15] It can also include a lock-key mechanism that allows it to be mounted onto a computer-controlled micropositioner (Fig. 1). During operation, the micropositioner submerges the MFP into the immersion liquid and precisely controls the gap 'G' between the mesa and the target substrate, maintaining a parallel configuration with a small separation distance, typically between 10 and 50 μm. Fluids are then injected and aspirated by applying positive and negative pressures, with effective confinement achieved when the ratio of aspiration to injection flow rates exceeds an experimentally validated threshold, which takes into account probe–surface gap variations, mechanical vibrations, configuration of the apertures, substrate uniformity, and flow-rate pulsations.

2.2 Hydrodynamic flow confinement (HFC)

HFC is a non-contact method that enables localized biochemical interactions on immersed biological substrates such as tissue samples and cultured cell monolayers on glass slides, Petri dishes, and microtiter plates.[21] It has evolved

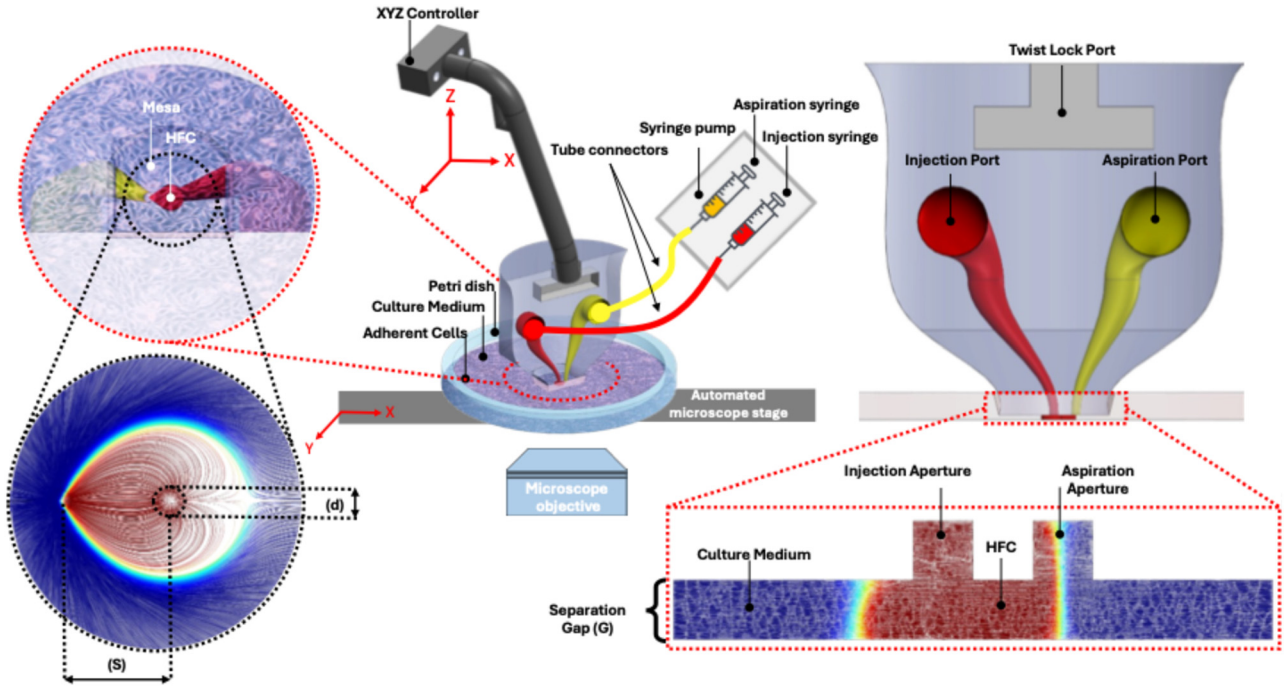

Fig. 1 The microfluidic probe (MFP) working principle, design, and experimental setup. (Center) Isometric schematic showing the integration of the MFP with an inverted fluorescence microscope. The probe holder is mounted on *XYZ* and angular controllers, connected *via* tight-fitted tubing to a programmable syringe pump. (Top-right) Side-view schematic of the MFP illustrating the injection and aspiration ports, extended channels, and the gap denoted as *G* formed between the MFP mesa and the bottom substrate. (Bottom-right) CFD-generated side-view image (zoomed) of the gap between the mesa and the bottom substrate, showing flow lines corresponding to the HFC, where the aspiration flow rate (Q_{asp}) exceeds the injection flow rate (Q_{inj}), resulting in complete confinement and re-aspiration of the injected fluid. (Top-left) Bottom view of the transparent working Petri dish, visualizing the HFC (red) generated by the MFP. (Bottom-left) CFD-generated bottom-view image (zoomed) showing flow velocity streamlines, coded with concentration values, beneath the mesa under HFC conditions ($Q_{asp} > Q_{inj}$), forming a confined tear-shaped flow pattern with complete re-aspiration. The aperture diameter is denoted as *d* and the center-to-center distance between apertures as *S*.

into a well-established technique in microfluidics, widely adopted across disciplines and technologies for its practicality and broad application potential. In a configuration known as Hele-Shaw flow, fluid is confined between two parallel surfaces under pressure applied through two or more fluidic apertures. At least one pair of injection and aspiration apertures is required to form a single HFC footprint, as shown in Fig. 1. This footprint can be scaled to operate on areas as small as individual cells or as large as entire tissue slices.

HFC relies on the immersion liquid, such as culture medium in a Petri dish, to surround and fully encapsulate a teardrop-shaped stream of processing fluid that is continuously injected and aspirated. This setup prevents mixing between the confined and surrounding fluids, allowing selective treatment of cells, subcellular regions, or tissue segments without affecting adjacent areas. To create this confinement, an MFP with at least two coplanar microapertures at the mesa is submerged in the immersion liquid and aligned parallel to the substrate at a gap below a defined threshold.[18] A pressure source, such as a syringe pump, is connected through tubing to the injection and aspiration ports, applying positive and negative pressures respectively. These opposing flows generate a confinement region with sharp, controllable boundaries that can take various shapes and sizes depending on the flow parameters.[22] The resulting flow remains in the laminar regime and is bounded by a stable fluid–fluid interface, producing a teardrop-shaped confinement zone. The simplest implementation, formed by two apertures, is commonly referred to as a flow dipole. Its characteristic shape includes a pointed side at the aspiration aperture and a curved side at the injection aperture, as shown in Fig. 1. Hitzbleck, Martina, *et al.* devised such a teardrop confinement zone,[23] using a microfluidic probe they developed, termed the "floating MFP", to produce hydrodynamic levitation for self-regulated distance control. By introducing a liquid flow between the probe and the sample surface at flow rates ranging from 5 to 500 μL min^{-1}, the system achieved stable levitation heights up to 15 μm without compromising probe performance.

2.3 Geometric and flow parameters

To successfully achieve HFC, a defined set of parameters must be controlled. Each application requires a specific confinement arrangement with a tailored shape and size. For example, when an MFP is used for surface patterning, the dimensions of the HFC area determine the shape and scale of the resulting "brush stroke", making precise control of the relevant parameters essential.[24] These parameters fall into two main categories: geometric parameters, which relate to

the design and spatial positioning of the MFP (including its vertical distance from the substrate), and flow parameters, which govern the behavior of fluid motion and depend on the properties of both the injected and immersion fluids. Geometric factors have a strong influence on the size of the HFC and on potential crosstalk when multiple aperture pairs are used, and they are defined during the design phase of the MFP. Flow parameters, in contrast, are more easily tuned during operation by adjusting the applied pressure through the control system. Both categories of parameters are typically analyzed using finite element method (FEM) simulations, followed by experimental validation to ensure reliable and reproducible confinement performance.

1 Geometric parameters. The geometric parameters of an MFP are dictated by the fabrication process used and the application of the MFP. Each fabrication technique has a specific resolution and a set of geometric limitations that control the geometric freedom of the MFP design. On the other hand, knowing the specific application of the MFP will determine the required number of HFCs, their sizes, their spatial configuration, and arrangement within the mesa of the MFP. By analyzing previous work,[13,25,26] it was found that the common set of geometric parameters controlling the design of an MFP is: a) the number of apertures and their spatial arrangement, b) aperture size and shape, c) separation distance between apertures of one pair S, d) the ratio between the distance separating a pair of apertures S and the diameter d of the apertures S/d, and finally e) the gap G between the MFP mesa and the bottom substrate, which is adjustable unlike other geometric parameters.

a) Apertures size, shape, and configurations. The MFP apertures size, shape, and their respective arrangements vary based on the sample size and intended application. Christ and Turner have analyzed the effect of apertures size on the shape of the HFC envelope.[27] Using four MFP devices with different aperture diameters while keeping all other geometric parameters constant, they showed strong agreement between experimental and computational results (Fig. 2(a)). Their analysis revealed that when the aperture diameter d is much larger than the apertures separation S ($S \ll d$), the HFC width w increases linearly with d, making aperture diameter the dominant parameter governing confinement size. In contrast, when $S \gg d$, the HFC width becomes insensitive to aperture diameter, and further changes in d do not significantly affect confinement. Quantitatively, the HFC remains strongly diameter-dependent when $S < 300$ μm, whereas for $S > 500$ μm, variations in d have minimal impact on the resulting flow envelope. In parallel, the cross-sectional shape of the apertures, whether square/rectangular,[28] circular,[16,29–32] or irregular, will further influence flow uniformity and confinement geometry.

With regards to configuration, the first reported MFP, as described in ref. 13, consisted of two adjacent apertures: one for injection and the other for aspiration. However, more complex configurations have also been developed for various applications. For example, in the work by Glia *et al.*,[29] cell capture was achieved using a single injection aperture arranged at the center of the MFP mesa, with another two aspiration apertures arranged in two crescent shapes at the periphery of the mesa. In the work described in ref. 33, a different arrangement of seven apertures was used to create six confinements. Six injection apertures were arranged radially with an aspiration aperture placed in the center. The MFP device enables rapid-switching open-space microfluidic display capable of delivering time-varying biochemical signals to cells across six independent confinement zones, enabling precise, multiplexed control of signaling inputs. A path toward understanding signaling dynamics.

Christ and Turner have analyzed the effect of apertures size on the shape of the HFC envelope.[27] Four devices with

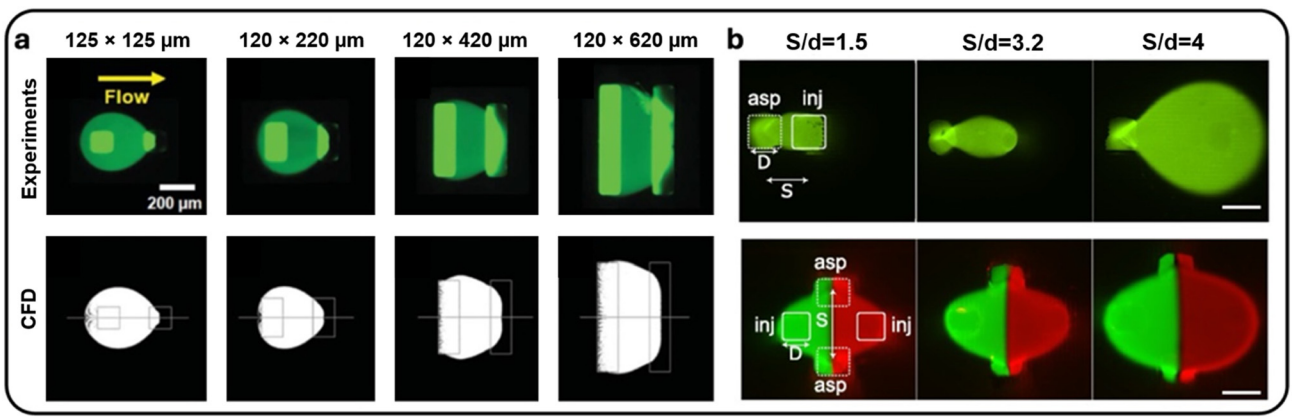

Fig. 2 The effect of aperture size and S/d ratio on HFC envelope in dipole and quadrupole configurations. (a) Characterization of the effect of aperture size on the HFC size, showing experimental panels (top) and computational simulations (bottom) flow envelopes for different aperture sizes. The panels show that the width of the envelope (HFC) increases with port size. Reproduced from ref. 27 with permission from *Lab on a Chip*, copyright 2011. (b) Characterization of microfluidic dipoles (top) and microfluidic quadrupoles (bottom) produced by 3D printed MFPs: (left to right) MD profiles produced using an MFP as a function of aperture spacing to diameter ratio (S_1/d), at Q_{inj} = 100 nL s^{-1}, α = 5. MQ profiles produced using an MFP as a function of S_1/d, at Q_{inj} = 100 nL s^{-1}, α = 3. Here, α represents the ratio Q_{asp}/Q_{inj}. All scale bars are 500 μm. Reproduced from ref. 16 with permission from *Scientific Reports*, copyright 2018.

varying aperture dimensions were studied while keeping other geometric parameters fixed. The experimental and computational HFC flow envelopes for the devices with varying aperture sizes are shown in Fig. 2(a). The main trend observed in both simulation and experimental was that HFC width w is linearly proportional to the aperture diameter d when the aperture-to-aperture separation S is much smaller than the aperture's width d. However, if S is much larger than d, then w becomes independent of d. It was also confirmed that the HFC size is highly dependent on the aperture's diameter for smaller separation distances, specifically, if $S < 300$ μm, the HFC size becomes highly dependent on the aperture diameter. However, for $S < 500$ μm, the HFC is less sensitive to the variations in aperture size. As for the shapes of the cross-sectional areas of apertures, they vary greatly and can be square/rectangular,[28] circular,[16,29–32] or other irregular, depending on the fabrication technique used and the intended application of the MFP.

b) Separation distance between apertures (S). Another important parameter that dictates the size of the HFC is the separation distance S between the two apertures of an injection–aspiration pair. This distance is measured from the center of one aperture to the center of the other. In the case of a dipole, the larger the distance between injection and aspiration apertures, the bigger the dipole formed.

The direct influence of S on the HFC width was investigated in ref. 27. It was found that for various aperture diameters, as the separation distance between apertures increases, so does the HFC footprint. Additionally, the separation distance dictates the size of the mesa. For example, in the same study, the size of the mesa was chosen based on the separation distance between the apertures of a single pair.[27] It was demonstrated that the mesa, in the context of planar MFPs, should be more than 10 times the spacing between the apertures to ensure flow confinement does not get affected by external conditions such as convection in the immersion liquid.

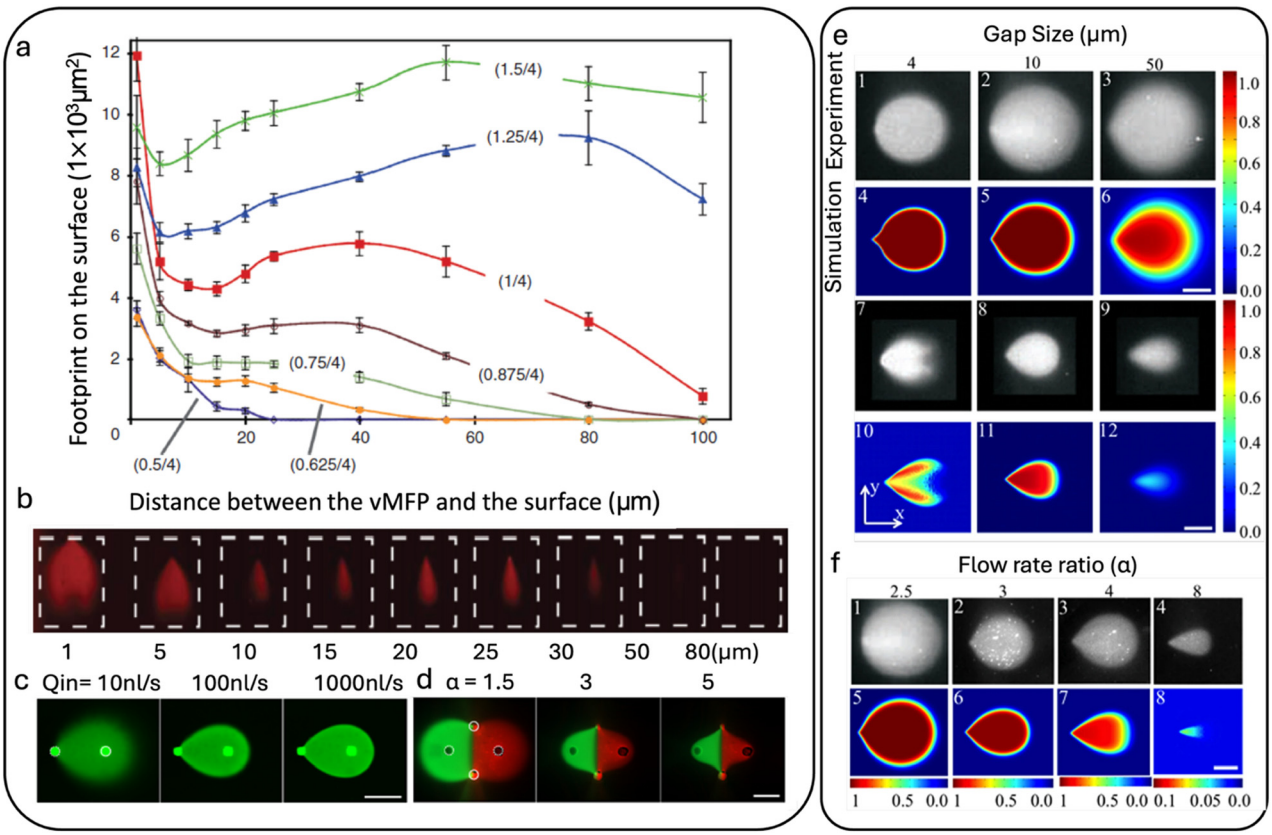

Fig. 3 The effect geometric and flow parameters on the HFC footprint. (a) The graph presents the areas of HFC footprints in square micrometer for different mesa to substrate gap distances and a set of injection to aspiration ratios α^{-1}. The injection and aspiration flow rates gradually varied from α^{-1} = 0.4/4 to 1.25/4 for gaps ranging from G = 1 μm to 80 μm. Reproduced from ref. 15 with permission from *Langmuir*, copyright 2011. (b) The evolution of footprints for fluorescently labelled antibodies on an activated glass surface for various distances between the vertical MFP head and the glass surface. Reproduced from ref. 15 with permission from *Langmuir*, copyright 2011. (c) The effect of varying injection flow rate on microfluidic dipole. Reproduced from ref. 16 with permission from *Scientific Reports*, copyright 2018. (d) The effect of varying flow rate ratio on microfluidic quadrupole. Reproduced from ref. 16 with permission from *Scientific Reports*, copyright 2018. (e) Experimental and simulation results demonstrating the effect of the gap. Reproduced from ref. 24 with permission from *Scientific Reports*, copyright 2015. (f) Flow rate ratio, α, and the injection flow rate, Q_{inj}, on the size and shape of the different HFCs. Reproduced from ref. 24 with permission from *Scientific Reports*, copyright 2015.

c) The ratio of separation distance to aperture diameter: S/d. In the preceding sections, the effects of the aperture diameter d and the aperture-to-aperture distance S on the HFC width w were investigated separately. However, according to the study described in ref. 16, the ratio between these two parameters, S/d, also affects the HFC footprint. In the experimental, numerical, and analytical characterizations that were performed, it was found that for a single dipole formed between two apertures, and for a quadrupole formed between four apertures, the higher the S/d ratio, the larger the area of the HFC generated. This trend can be seen in Fig. 2(b) for dipoles and quadrupoles, respectively.

d) Gap between the mesa and the substrate: G. The gap G is the distance between the mesa of the MFP and the bottom substrate on which the sample resides, and it is an important parameter that determines the shape and size of the HFC, as well as the resulting shear stress on the substrate. During the experiment, this parameter can be computer-controlled by a micropositioner to which the MFP is connected.

In the vertical microfluidic probe (vMFP) work,[15] the effect of the gap G on the area of the HFC was investigated. A graph of the footprint of the HFC for different mesa-to-substrate gap distances and a set of injection-to-aspiration flow rate ratios α^{-1} was presented, as shown in Fig. 3(a). The footprint was assessed using fluorescence microscopy by visualizing the pattern of antibodies deposited on a glass-bottom substrate. The MFP head used in these experiments had two square apertures with a lateral dimension of d = 50 μm and a separation distance between them (center-to-center) of S_1 = 50 μm. It can be observed from the graph and the fluorescent footprints that for a fixed flow-rate ratio, the relationship between the gap size and the HFC footprint is non-linear and widely varies at different ranges of gaps and for the different flow rate ratios Fig. 3(b) and (e). For the gap sizes between 1 and 5 μm, as the gap size increases, the HFC size decreases sharply for all flow rate ratios. On the other hand, for gap distances between 10 and 20 μm, the footprint of the HFC is not significantly affected. The HFC footprint shrinks as the gap increases from 20 to 25 μm for the lower flow rate ratios (higher α^{-1}). For high flow ratios, $\alpha > 4$, with larger gaps, $G > 40$ μm, the HFC footprint size significantly drops or disappears. This graph serves as an experimental characterization reference for MFPs with similar dimensions. In another work by Safavieh *et al.*,[34] the influence of the gap size on the HFC footprint was presented by measuring the minor and major axes of the HFC teardrop-shaped region as seen in Fig. 3(e). It was found that for a fixed flow rates ratio and $1 < G < 50$ μm, the larger the gap size, the smaller the HFC size (stronger confinement).[24] Also, the variation in confinement lengths was linearly proportional to the gap sizes of the MFP.

The gap size not only affects the size of the HFC but also plays a direct role in determining the shear stress within the confinement between the mesa and the substrate, where the sample under study lies. To maintain the integrity of the sample, whether adherent cells or tissue slices, it is essential to investigate the effect of shear stress on cells as a result of variations in gap size. In the same work described above,[24] the effect of the gap size on the shear stress was also investigated. It was found that the two are inversely proportional, where shear stress decreases exponentially as the mesa moves away from the substrate.

Additionally, since the MFP is used for applications such as cell dissociation, it is important to know the safe range of shear that allows for detaching cells while maintaining their integrity. The range of shear stresses (τ) for which a cell can be safely detached without membrane damage is commonly reported to lie between 0.5 and 1.5 Pa for endothelial cells.[35,36] However, this threshold is not universal across cell types. For example, tumor cells *in vivo* experience shear stresses of 0.05–0.4 Pa in venous flow and 0.4–3 Pa in arterial flow, with some studies reporting exposure up to 3 Pa or higher during transit.[37] Experimental work further shows that B16 melanoma cells remain viable under shear rates up to ~300 s^{-1}, with significant loss of viability occurring only beyond this range.[38] The shear stress value is calculated as shown in eqn (1).[39]

$$\tau = \mu \cdot \mathrm{d}u/\mathrm{d}y \quad (1)$$

The flow underneath the mesa becomes faster as the gap becomes smaller, according to the principle of conservation of mass, as shown in eqn (2).

$$Q_{\mathrm{tot}} = A \cdot u \quad (2)$$

where μ is the dynamic viscosity, A is the cross-sectional area through which the fluid flows, and u is the velocity of the fluid parallel to the substrate. The gap represents the height of the cross-sectional area in the y-direction, and as the gap becomes smaller, so does the area, for a constant flow rate Q

2 Flow parameters. Following the design and characterization of the geometric parameters of the MFP, flow parameters are selected to ensure safe and effective operation with biological samples. Unlike geometric parameters, flow parameters can be controlled during experimental characterization. Manipulation of the size, shape, and intensity of the generated HFC is possible by controlling the flow parameters. By analyzing previous work, it was found that the main flow parameters affecting the flow are the injection flow rate, Q_{inj}, aspiration flow rate, Q_{asp}, and their ratio, $\alpha = Q_{\mathrm{asp}}/Q_{\mathrm{inj}}$. All flow rates are manipulated by computer-controlled pressure sources such as syringe pumps.

1. Injection (Q_{inj}) and aspiration (Q_{asp}) flow rates. MFPs can come with various numbers of injections and aspiration apertures that connect to fluid flow or pressure sources. Controlling these parameters enables precise, real-time control of the HFC. By increasing Q_{inj} and Q_{asp} simultaneously, while maintaining a constant ratio α, the sharpness of the HFC edges can be increased with minimal variations to its shape or size. Thus, the footprint of the HFC

is independent of the absolute values of the injection and aspiration flow rates.[16] For example, it was experimentally demonstrated that by keeping α constant, the HFC footprint transitions from a hazy to a more sharply defined shape as the injection flow rate increases, as shown in Fig. 3(c).

2. Flow rates ratio: $\alpha = Q_{asp}/Q_{inj}$. The flow rates ratio $\alpha = Q_{asp}/Q_{inj}$ has been one of the most studied parameters in previous work due to its significant effect on the size and shape of the HFC.[16,31] In the foundational MFP study,[13] the HFC size was initially investigated under different flow rate ratios (ranging from 2.5 to 16) at Q_{inj} = 0.44 nL s^{-1}. In a follow up work, the influence of the flow rates ratio on the HFC shape and size was investigated for 3D printed MFPs.[16,31] This phenomenon was observed with both the dipole and quadrupole[16] configuration, where the footprint becomes both smaller and more defined, and in this case, due to higher flow rate ratio and injection flow rate, respectively, as shown in Fig. 3(d and e). In practice, the flow-rate ratio (α) is the dominant factor governing the size and sharpness of the HFC boundary. However, in specific operating regimes, such as at very low flow-rate ratios, in specialized configurations like the microfluidic quadrupole, or when performing a diffusion-driven flow inside tissues, the diffusion coefficient of the analytes can play a more pronounced role in shaping the effective confinement interface. In conclusion, to change the size of the HFC, one must control the flow rates ratio α or the separation distance S_1 between two apertures as discussed in the previous section. Table 1 summarizes all the geometric and flow parameters controlling the HFC that have been analyzed in the literature.

2.4 Fluid mechanics of MFPs

Fluid flow is driven by pressure difference, gravity, or externally applied forces. To design an MFP that manipulates fluids precisely, it is crucial to understand fluid mechanics at the microscale. Fluid mechanics is dedicated to studying fluid behavior at rest and in motion.[40] Fluids include all materials that have the tendency to flow and deform continuously under the application of shear stress such as liquids, gases, blood, and plasma. In the specific application of an MFP, the processing fluid undergoes two different boundary conditions (BC). The first BC occurs during the flow of fluid through the closed channels inside the MFP during injection and aspiration. The second BC arises once the fluid exits the apertures and flows between the MFP mesa and the substrate. This region forms a thin liquid layer confined between two parallel plates and is well described by Hele-Shaw theory.[41] In such shallow geometries, as originally demonstrated by Hele-Shaw, the resulting 2D fluid flow streamlines are analogous to the streamline produced by 2D electric fields. This analogy was exploited to "simulate" electric fields in complex capacitor geometries in an era where numerical simulation tools were absent.[42]

During flow out of the apertures into the gap underneath the mesa, boundary conditions involve two parallel surfaces in close proximity that confine the fluid. This phenomenon is termed the Hele-Shaw flow, and was first introduced by Henry Selby Hele-Shaw in 1898.[41] The sections below outline key physical principles such as flow confinement, shear stress, and transport behavior, which are essential for designing and operating microfluidic probes. Visualizing and understanding the properties of the working fluid during its journey from the syringe to the MFP, through open space, and back into the MFP is vital for designing and utilizing this novel tool. It enables the quantification of the dominant forces, flow velocity, wall resistance, pressure, shear stress, advection, and diffusion, all of which are major properties influenced by the biological samples under study. For example, identifying wall shear stresses enables successful cell stimulation and/or dissociation experiments without jeopardizing cell integrity.

Boulais and Gervais have presented a 2D microfluidics cookbook to explain the physics of the HFC by modeling it as a type of Hele-Shaw flow. Using analytical tools such as potential flow, conformal mapping, and convection–diffusion modeling, they provided a framework to predict reagent confinement, mixing, and transport in plane flow devices. This contribution is valuable in MFP applications since it offers a rigorous and practical guide to designing HFC geometries that achieve robust micrometer-scale confinement that achieve efficient reagent delivery without physical walls.[42]

1 Navier–Stokes equation and the Hele-Shaw flow. HFC is best understood by going back to the roots of its discovery by the scientist Henry Selby Hele-Shaw. He invented a method that enabled the visualization of streamlines of a flow by

Table 1 Geometric and flow parameters controlling the HFC

Type of parameter	Parameter	Symbol/abbreviations
Geometric	Number of aspiration and injection apertures	N_{asp}, N_{inj}
	Gap between mesa and substrate	G
	Aperture diameter	d
	Center-to-center distance between a pair of apertures	S
	Ratio of aperture spacing to diameter	S/d
Flow	Injection flow rate	Q_{inj}
	Aspiration flow rate	Q_{asp}
	Flow rate ratio (aspiration to injection)	$\alpha = Q_{asp}/Q_{inj}$
	Diffusion coefficients of injected fluid	D

confining fluids between two parallel and closely spaced plates naming the device the Hele-Shaw setup. The flow between the plates is laminar at all velocities and is generally a class of quasi-two-dimensional (2D) flow. It can be described with a single scalar function from which all flow properties can be calculated. In this sense, Hele-Shaw flow fields bear a strong mathematical analogy with electrostatic, magnetostatic, and gravitational fields.

Deriving the Hele-Shaw equation starts from the general, nonlinear, vectorial, time-dependent partial differential equation (PDE), namely the Navier–Stokes equation (NSE) for incompressible fluids. The solutions of this equation describe all possible physical cases in laminar fluid dynamics for the given initial and boundary conditions used. The NSE in the absence of external forces other than pressure is given as in eqn (3).[43]

$$\rho\frac{\partial\vec{v}}{\partial t}+\rho\vec{v}\cdot\vec{\nabla}\vec{v}=\mu\vec{\nabla}^2\vec{v}-\vec{\nabla}p \tag{3}$$

where ρ is the fluid density, μ is the dynamic viscosity, p is the pressure distribution, and $\vec{v}$ is the 3D velocity vector field. For the specific case of an HFC, some assumptions are made to simplify the Navier–Stokes equation to the Hele-Shaw equation. It is assumed that the gap between the parallel plates is much smaller than the characteristic length over which HFC occurs $G^2/L^2 \ll 1$. Also, the Reynolds number must be much smaller than 1 (Re $\ll$ 1), which is valid for all microfluidic flows. Additionally, the flow should be purely creeping, which holds for flow between parallel plates over long-distance L. Finally, the pressure gradient in the direction perpendicular to the flow must be negligible ($\partial p/\partial z \rightarrow 0$), a condition that is typically satisfied in microfluidic systems.

When the separation thickness d in the z-direction is much smaller than the lateral dimensions of the flow, the system behaves as a quasi-two-dimensional fluid domain, as described in eqn (4).

$$u=\frac{-1}{2\mu}\cdot z(d-z)\left(\frac{\partial p}{\partial x}\,\hat{x}+\frac{\partial p}{\partial y}\,\hat{y}\right) \tag{4}$$

where p is the scalar pressure, and $\hat{x}$ and $\hat{y}$ the unit vectors in the x and y directions. This corresponds to a parabolic velocity distribution in the z-direction modulating an irrotational 2D flow field in the x, y plane. As shown by Boulais and Gervais,[42] The 2D flow can be described by a potential function Φ, which in the absence of sources or sinks satisfies Laplace's equation (5):

$$\nabla^2\Phi=0 \tag{5}$$

In this framework, flow in a Hele-Shaw cell can be modeled using potential theory, which is mathematically analogous to the analysis of 2D electric fields. This correspondence allows us to apply the full suite of classical electrostatics tools to characterize flow behavior in microfluidic systems.[42]

2 Flow, transport, and shear dynamics in Hele-Shaw microfluidics. In Hele-Shaw configurations, relevant to the HFC produced by the MFP, and similar to classical microfluidics, flow behavior, mass transport and shear stresses are governed by a set of characteristic dimensionless numbers, such as Reynolds and Péclet's numbers. However, because the gap height between the probe and substrate is significantly smaller than the lateral dimensions, momentum and mass transport follow Hele-Shaw scaling laws rather than classical channel flow behavior. Table 2 summarize these key parameters, which define this unique microscale regime.

Reynolds number (Re) is the non-dimensional parameter, that helps predict fluid flow patterns by expressing the ratio of inertial forces to viscous forces. At low Re, flows tend to be dominated by laminar (sheet-like) flow, while at high Re, flows tend to be turbulent. In Hele-Shaw configurations, the Reynolds number deviates from the classical pipe-flow expression because the gap height (H) is much smaller than the lateral dimensions. Under these conditions, inertial effects scale with H^2 and the appropriate form of the Reynolds number is:

$$\mathrm{Re}=\frac{\rho UH^2}{\eta S} \tag{6}$$

where U is the in-plane flow velocity, H the gap height, S the inter-aperture distance, and η the dynamic viscosity. This expression captures the dominance of viscous dissipation between two closely spaced plates.

Mass transport within a HFC reflects a balance between convection and diffusion. In MFP systems, the Péclet number depends strongly on α, as given by the expression from Safavieh *et al.*:[24]

Table 2 Summary of key dimensionless numbers in open-space microfluidics

Quantity	Expression (Hele-Shaw)	Key parameter	Typical values (MFP)
Re	$\frac{\rho UH^2}{\eta d}$	Inertial effects scale with H^2	0.001–0.01
Pe	$\frac{Q_{\mathrm{inj}}}{8\pi DG}\frac{(\alpha-1)^3}{\alpha}$	Strongly dependent on α	10^2–10^3 (convection-dominated)
R	$\frac{8\mu\cdot L}{\pi r^4}$	Dependent on r^4	10^9–10^{11} Pa s m^{-3}
τ	$\mu\left(\frac{\partial\lvert u\rvert}{\partial z}\right)_{z=0}$	Velocity gradient in the z-direction	<2 Pa

$$\mathrm{Pe} = \frac{Q_{\mathrm{inj}}}{8\pi DG}\frac{(\alpha-1)^3}{\alpha} \tag{7}$$

where Q_{inj} is the injection flow rate, D the diffusion coefficient, and G the geometric conductance of the Hele-Shaw gap. In a typical HFC, the flow satisfies the Hele-Shaw approximation. It's characterized by a low Reynolds number ($\mathrm{Re} \ll 1$) and a high Péclet number ($\mathrm{Pe} \gg 1000$). Under these conditions, viscous forces overwhelmingly dominate inertial effects, and convective transport far exceeds diffusive mixing.[42]

In closed channels, fluidic resistance is imposed on the fluids by the internal walls with flows inside microchannels experiencing greater resistance than those in larger channels. This resistance imposed on the fluid by the internal channel walls is highly analogous to the resistance that electric wires impose on the flow of electrons. Analogous to Ohm's law, the Hagen–Poiseuille's law can be derived for fluidic resistance, as shown in eqn (8).[44]

$$\Delta P = R{\cdot}Q \tag{8}$$

where ΔP is the pressure drop, Q is the volumetric flow rate, and R is the hydraulic resistance, which correspond to the voltage drop, current, and electric resistance, respectively. The resistance that a fluid of viscosity u experiences as it passes through a channel of length L and radius r is given by the simplified form in eqn (9).[44]

$$R = \frac{8\mu{\cdot}L}{\pi r^4} \tag{9}$$

3 Shear stress under the HFC. Biological samples positioned under the MFP mesa experience shear stresses. Because cells and tissues have finite shear-tolerance limits, accurately characterizing these stresses is essential to avoid detachment, deformation, or lysis. In a Hele-Shaw configuration, shear stress at the substrate is determined by the velocity gradient in the z-direction:[42]

$$\tau = \mu\left(\frac{\partial|u|}{\partial z}\right)_{z=0} \tag{10}$$

Since the velocity field in a Hele-Shaw cell is the product of a parabolic profile across the gap and a 2D potential flow, the shear stress becomes directly proportional to the local 2D flow field.[42] Thus, any 2D potential-flow solution describing the HFC also defines its shear-stress map.[42] Regions of highest 2D velocity, *i.e.* near the injection and aspiration apertures, correspond to the highest shear stresses. Although ideal point-source models diverge at the aperture center, real apertures have finite size; accurate shear estimates are obtained by evaluating the 2D velocity field at a radial distance equal to the aperture radius.

In the work by Queval *et al.*,[45] the main parameters affecting shear stress were shown to be the injection and aspiration flow rates and their ratio, the diameter of the apertures, and the gap size. Another important aspect of shear stress that directly contributes to how it affects cells is the mode of flow application: whether it is intermittent or continuous. A lower continuous shear rate is more likely to dissociate cells than a higher intermittent shear rate. In the case of dissociated neurons, one study showed that cells can withstand stresses of up to 1.5 Pa when applied intermittently for periods of 2 h, although they detach under stresses of 0.5 Pa when applied continuously.

2.5 Hydrodynamic multipoles

HFCs can take on various shapes, sizes, and symmetries, and may consist of different numbers or arrangements of dipoles, collectively referred to as hydrodynamic multipoles. The concept and terminology of microfluidic multipoles were first formalized by Goyette *et al.*,[46] where dipoles, quadrupoles, and higher-order configurations were shown to be generated and analyzed using conformal mapping, and described both rotational and translational symmetries relevant to open-space microfluidics, see Fig. 4(a). While HFC is theoretically achieved when $\alpha > 1$, the effective threshold in experiments depends on system-specific operational factors. As a result, stable HFC often requires moderately high α *values*, with reported experimental values ranging from 1.5 to 3 in geometries that benefit from additional stability margins. Therefore, the optimal operating α must be experimentally verified for each setup and configuration.

1 Microfluidic quadrupoles (MQ). Microfluidic quadrupoles occur when an MFP has four apertures at its mesa. The apertures of an MQ can either be aligned along a straight line and are then called linear quadrupoles, or arranged at the corners of a rectangle and are then termed lateral quadrupoles.[18] In both configurations, each injection aperture is adjacent to an aspiration aperture, with the linear arrangement having the injection apertures on the inner side. A typical quadrupole is shown in Fig. 4(a). The influence of geometric and flow parameters on quadrupoles resembles their effect on MDs: as S/d increases and α decreases, the HFC area of the MQ expands. Conversely, as the ratio between aspiration and injection rates α increases while maintaining Q_{inj} = 100 nL s^{-1} and S/d = 5.5, the HFC footprint becomes smaller, as shown in Fig. 3(d).

2 Microfluidic pixels. Microfluidic pixels are a unique type of polygon-based microfluidic multipoles. The pixelated chemical display (PCD) was first presented by Goyette *et al.*[47] The concept suggests that the injection aperture is located at the center of the pixel, and the aspiration apertures are positioned on the vertices of a polygon at the periphery of the pixel. Microfluidic pixels adjacent to one another share aspiration apertures on their vertices to form a lattice of apertures, which for certain regular polygonal shapes, can completely tessellate

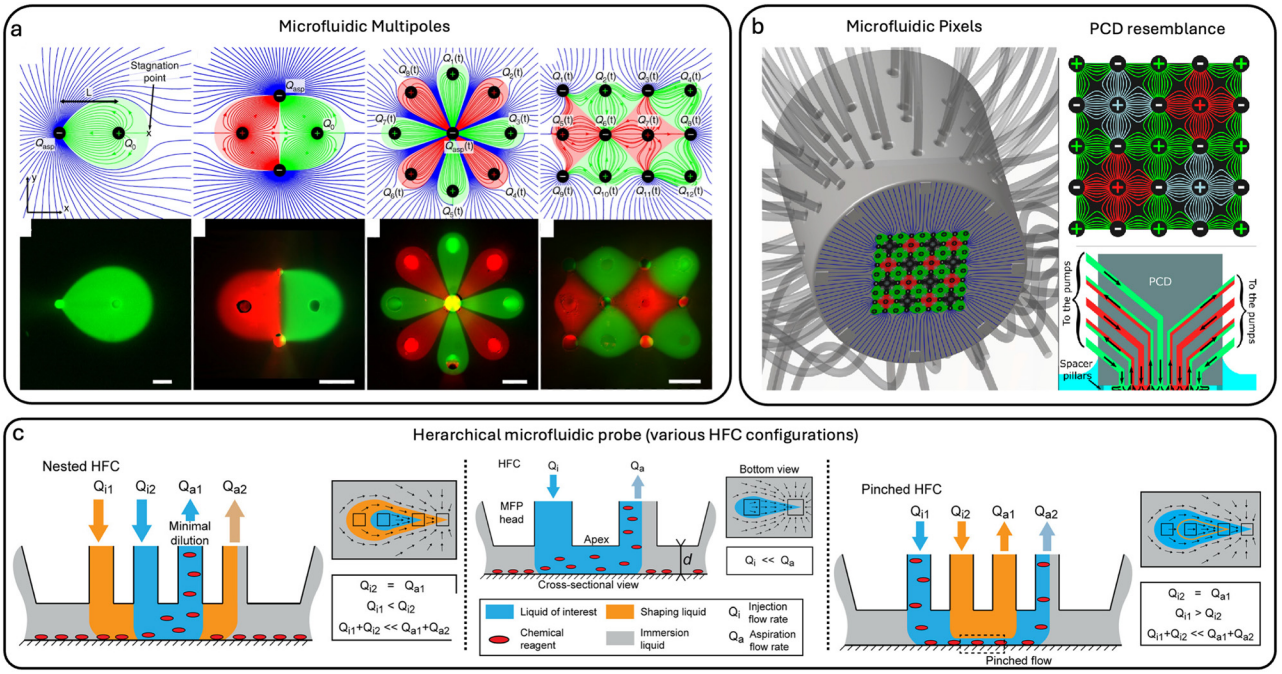

Fig. 4 Microfluidic multipoles. (a) Theoretical flow streamlines (top) are shown alongside corresponding fluorescence images (bottom). Injection and aspiration apertures are indicated by positive and negative symbols. Panels from left to right illustrate a microfluidic dipole, quadrupole, multipole configuration with rotational symmetry, and translational symmetry. Scale bars = 500 μm. Reproduced from ref. 46 with permission from *Nature Communications*, copyright 2019. (b) Schematic of PCD concept using an MFP with multipoles. The MFP is equipped with an 8-aperture square-pixel PCD. The model shows multiple tube connections. (Top right) Theoretical flow lines in an array of microfluidic pixels under a PCD. Positive and negative signs representing injection and aspiration apertures, respectively. (Bottom right) Side-view cut schematic of the PCD-MFP. The PCD is maintained at a fixed height above the surface using spacer pillars. Fluids are injected and aspirated within the gap between the device and the surface. Reproduced from ref. 47 with permission from *Applied Physical Sciences*, copyright 2020. (c) Principle of hierarchical HFC. In the classical HFC (middle), a processing liquid (blue) is confined, in the presence of an immersion liquid, between the MFP mesa and the surface. (Left) The addition of a shaping liquid (orange) and setting the injection and aspiration flow rates of the liquids appropriately enables nested HFC or (right) pinched HFC for efficient use or recovery of chemicals during local surface processing. Reproduced from ref. 48 with permission from Langmuir, copyright 2014.

a surface with independent and isolated fluid confinement areas (Fig. 4(b)). The architecture of pixelated devices is highly modular as any number of columns or rows of microfluidic pixels can be added along the periphery without affecting the inner units. Inside a single pixel, reagents are primarily transported by convection, and although diffusion into neighbouring pixels can occur, its extent is governed by the same parameters as in traditional microfluidic probe operation, such as flow rate and molecular diffusion coefficient, and is not inherently greater in pixelated configurations (Fig. 4(b)).[47]

3 Hierarchical HFC (h-HFC). In an ordinary HFC, there are two fluids, the processing fluid which is injected from one of the apertures, and the immersion fluid covering the substrate in which the MFP is submerged. On the other hand, in a hierarchical HFC, an extra pair of apertures is introduced. The new set of apertures consists of an injection aperture and an aspiration aperture placed on the two outer sides of the original apertures and usually has larger dimensions. These newly introduced apertures are used to inject a shaping liquid to envelop the processing liquid of interest within the shaping layer. The final shape of the confinement entails multiple layers of shaped liquids confined within the immersion liquid to process a target area of the substrate of interest,[48] see Fig. 3(c). The relationship between the injection and aspiration flow rates is distributed unequally between the processing "nested" liquid and the intermediate (shaping) liquid, without affecting the stability of the flow confinement. In the work by Huber *et al.*,[49] an MFP was used to develop an h-HFC to localize liquids on cytological samples.

4 Deep-reaching HFC. In the work by Oskooei *et al.*,[21] a deep-reaching-HFC (DR-HFC) was devised as a simple, passive, and reliable hydrodynamic confinement concept. Two probe configurations are presented: linear and annular, and both comprise a reagent-injection aperture and aspiration apertures that confine the injected reagent. The linear DR-HFC consists of an injection aperture in the middle bordered by two aspiration apertures, whereas the annular configuration consists of an injection aperture surrounded by an annular aspiration aperture. Deep-reaching confinement is achieved due to the symmetric aspiration of the injected liquid reagent, which enables the reagent to penetrate to a larger depth before it is collected by the aspiration apertures, without the need for high flow rates.

3 Microfabrication techniques for MFPs

MFPs have evolved significantly through advancements in microfabrication techniques, which determine their structure, resolution, material properties, and functional capabilities. Early MFPs relied heavily on cleanroom-based methods such as photolithography and deep reactive ion etching, which offered high precision but involved costly and time-intensive processes. These were followed by soft lithography approaches that simplified fabrication, improved accessibility, and reduced production costs. More recently, 3D printing technologies have enabled unprecedented design flexibility and integration potential. The following sections highlight key fabrication strategies, along with their advantages, limitations, and the types of MFPs they enable.

3.1 Photolithography and deep reactive ion etching

Photolithography, a key technique that emerged in the semiconductor industry in the early 1960s, was later widely adopted in micro-electro-mechanical systems (MEMS), paving the way for the development of microfluidic chips decades later. This process involves projecting a pattern from a lithographic mask onto a photosensitive resist applied to a substrate, followed by deep reactive ion etching (DRIE). In microfluidics, DRIE is used to create channels with high-aspect-ratio features.[50] The first MFP ever fabricated was produced using this method, and over the past two decades, various MFPs have been made using this technique.[13]

An example of an MFP fabricated using this technique is described in ref. 14, where a square silicon (Si) chip is fabricated from a 200 μm thick, double-side-polished Si wafer using photolithography and DRIE. Etching masks were formed on Si wafers with S1813 photoresist to pattern a 2 μm thick thermal SiO_2 layer. In another work,[15] vertical MFP heads were composed of a 400 μm thick Si layer holding microfabricated structures bonded with a 500 μm thick glass layer. The microchannels and vias were made in a 4-inch Si wafer using standard photolithography with a photo-plotted mask and DRIE. Despite this technique's great advantages, including high precision and versatility, it has some significant disadvantages such as long lead time, processing time and high associated costs. These require bulk micromachining of the MFP's Si chip, PDMS block fabrication using soft lithography, precise alignment and assembly of layers, and separate machining of the probe holder.[13,45]

In the work by Jiang *et al.*, selective laser-assisted etching (SLE) was used to fabricate a monolithic MFP that is robust and accessible, eliminating wafer bonding and reducing polishing steps for mass spectrometry imaging of tissues.[51] The work by Kim *et al.*, an advancement in SU-8 photolithography was demonstrated through a novel dry thermal-release fabrication process enabling batch production of free-standing microfluidic probes. This method simplifies probe release while allowing integration of functional elements such as metal thin-film electrodes for impedance sensing, enhancing device versatility for bioengineering applications.[52]

Despite the intricacy of these techniques, their limitations and sophisticated fabrication techniques led to the development of a derivative fabrication technique, namely soft lithography, which reduces major steps to save time, cost, and effort.

3.2 Soft lithography

One of the major fabrication techniques in microfluidics in recent years is soft lithography, a microfabrication method first introduced by Qin *et al.* in 2010.[53] The technique primarily involves casting a polymer and then bonding it to a glass slide in a series of steps. It begins with designing and fabricating a mold using conventional photolithography. Alternatively, master molds can also be fabricated using high-resolution 3D printing, which enables rapid and cost-effective pattern generation without requiring access to a cleanroom. Then, a molding step follows, in which PDMS-based microfluidic devices are created by casting the polymer against the mold. This is followed by bonding the PDMS layer to a glass slide.

Soft lithography begins with the microfabrication of a master mold. This process starts by transferring a computer-aided design (CAD) layout onto a Si wafer, typically performed in a cleanroom using standard photolithography on photosensitive resins. The CAD model is first written onto a photomask using a laser writer. In the next step, the pattern on the mask is transferred to a substrate (usually glass or Si) by coating it with a thin layer of photoresist. Light of a specific wavelength is then projected through the mask onto the photoresist, imprinting the design onto the substrate. After the photoresist is developed, the resulting patterned substrate becomes the master mold. It is important to note that soft lithography does not inherently depend on photolithography; 3D printed molds have increasingly become a viable alternative for producing microscale features, particularly when high-resolution 3D printers are available. The master mold can then be reused for repeated PDMS molding.

Once the master mold is ready, the soft lithography process begins. This technique transfers the design from the master mold onto PDMS to create a microfluidic device. It starts by preparing the PDMS material through mixing two components: the base and the curing agent. Before casting, the master mold is treated with a silanization step to modify its surface and facilitate easy peeling of the PDMS after curing. The PDMS mixture is then poured onto the mold, followed by degassing to remove air bubbles, casting, and curing to harden the material. After curing, the PDMS is

peeled from the mold and bonded to a glass slide using oxygen plasma. Soft lithography remains widely adopted because of its low cost, rapid prototyping capability, biocompatibility of PDMS, and its ability to generate multilayer or moderately complex microfluidic structures with high fidelity. Soft lithography offers several advantages over traditional photolithography: it reduces lead time and processing steps, and enables multiple devices to be fabricated from the same mold, making it ideal for rapid prototyping and iterative testing. An example of an MFP fabricated using soft lithography is presented in ref. 45, which describes a microfluidic system incorporating a perfusion chamber and a novel transparent MFP for localized micro-perfusion of brain tissue. The MFP, fabricated using PDMS, features six micrometer-scale apertures and can be assembled within a few hours in a standard laboratory. It was successfully used for perfusing a small number of cells in a brain slice with concurrent confocal fluorescence imaging of the perfused dye. However, the main challenge encountered with this PDMS-based MFP was the alignment and bonding of the different layers.

Despite the advantages that this major fabrication technique for classical closed-channel microfluidic devices brings to MFPs, it also presents several drawbacks. The primary limitation lies in the difficulty of aligning multiple PDMS layers, which complicates the fabrication of precise aperture sizes and arrangements. Moreover, soft lithography relies on molds produced using standard photolithography, a process that requires expensive cleanroom facilities and specialized technical staff. The technique is also constrained to 2D and 2.5D geometries, limiting the development of innovative MFPs with complex structures and customized aperture configurations. These limitations have driven the emergence of 3D printing as a powerful alternative. Unlike traditional methods, 3D printing offers significantly greater design flexibility by enabling full three-dimensional fabrication.

3.3 3D printing

Three-dimensional (3D) printing is a manufacturing method that uses computer-aided designs to build structures layer by layer.[54] With the advancement of these technologies, it has become a widely used approach for fabricating microfluidic devices. The fabrication of MFPs using 3D printing offers several advantages, including the ease of performing mass customization, facilitating design modifications, and implementing updates at low cost compared to common microfabrication techniques. This reduces both the time and cost required. Other benefits include decentralization of manufacturing, reduction in repair time, lower labor costs, and faster time to market, all without compromising the ability to fabricate high-complexity structures.[55] Crucially, by gaining the third dimension, 3D printing enables the development of innovative and integrative MFPs.

MFPs were first 3D printed using stereolithography (SLA), a technique that cures liquid photopolymer in a vat using light-activated polymerization.[16] The process begins by lowering the build platform into a vat containing photosensitive resin. The model is printed layer by layer, line by line, or even point by point, by projecting ultraviolet light from a projector or laser source, which induces a reaction that solidifies the resin. Once the part is complete, the resin is drained, and the solidified structure is removed. Materials used in vat photopolymerization vary depending on the process and include tough, flexible, transparent, and castable photopolymer resins. Several 3D printing technologies fall under this category, with the most common being SLA, digital light processing (DLP), and carbon digital light synthesis (CDLS).

The first 3D printed MFP was designed featuring two models: an MFP with built-in reservoirs and twist-lock mechanisms for probe-holder connections, and a simpler design with glued fluidic connections instead of a reservoir. These MFPs generated dipolar and quadrupolar HFCs and were tested for biocompatibility through cell-staining experiments.[16] Advancements in 3D-printed probes led to integrated MFPs like the micro-electro-fluidic probe (MeFP), which uses dielectrophoresis (DEP) for selective cell capture and dynamic cell patterning.[56] Another development is the multiphysics MFP, which incorporates electro-heating elements and high-resolution microfluidic injection for single-cell manipulation and targeted drug delivery.[31] Additionally, the noncontact multiphysics probe (NMP) combines electro-permeabilization, hydrodynamic flow confinement, and contactless scanning, allowing for precise macromolecule delivery and repeatable nano-biopsies on single viable cells.[31] Furthermore, the herringbone microfluidic probe (HB-MFP) was developed for high-throughput sample processing and capturing of circulating tumor cells (CTCs) from whole blood samples. The HB-MFP integrated radial herringbone elements on its mesa to generate microvortices, allowing for efficient capture and downstream characterization of CTCs from cancer patients' blood samples.[29] All these MFPs were possible due to 3D printing technology, which gave flexibility for highly complex and customized designs with integrated features, rapid prototyping, and minimal assembly, consequently enhancing performance and reducing costs.

3.4 Stainless steel stacking

In addition to flexibility in design, flexibility in material selection is also key to unlocking new opportunities for MFP development. For instance, a stainless-steel MFP (stMFP) was developed to create a two-dimensional aperture array with narrow spacing.[57] The motivation behind developing stainless steel MFPs was to enhance local processing and enable high-density biopatterning by designing a multi-aperture MFP capable of expanding a 2D aperture array at narrow intervals. Traditional MFPs made from Si-glass or

PDMS are often limited in aperture density due to the difficulty of fabricating closely spaced channels. Stainless steel substrates offer more flexibility in arranging apertures in 2D, supporting advanced applications in tissue engineering, biosample stimulation, and 3D gel structure formation, thereby overcoming the limitations of conventional materials and fabrication methods.

In this stacking-based fabrication method, the thin stainless-steel substrates are patterned by photolithography and wet etching to create two functional layer types: partition layers containing port openings, and microchannel layers containing etched flow pathways.[57] These layers are then precisely aligned, stacked in an alternating sequence, and diffusion-bonded to form a monolithic structure with individually addressable apertures connected through isolated microchannels. This method avoids the need for complex 3D microchannel architectures and enables straightforward scalability simply by increasing the number or arrangement of stacked layers. After bonding, the probe's distal surface is polished to expose a clean and uniform aperture array. Owing to the rigidity and chemical resistance of stainless steel, the device can withstand aggressive cleaning protocols and be reused after experiments involving biological samples, making it a durable and versatile platform for high-density open-space microfluidic operations.[57]

The stMFP was then applied to demonstrate high-resolution biopatterning, enabling precise deposition of fluorescent antibodies across a variety of controllable 2D treatment patterns. By independently addressing apertures within the dense array, the device produced multiple isolated patterns and complex multi-component arrangements, demonstrating its ability to perform localized surface treatments at high spatial density. These results highlight the stMFP as a powerful tool for advanced bioprocessing applications requiring fine spatial control over chemical delivery.[57] However, the fabrication of steel layers requires labor-intensive processes involving precise alignment and bonding of the different layers.

Beyond common fabrication methods like photolithography, soft lithography, 3D printing, and stainless-steel stacking, thermoplastic microfabrication is emerging as a cost-effective approach for MFPs. Using materials such as cyclic olefin copolymers, these methods enable rapid, low-cost production through thermal moulding and bonding, avoiding the need for cleanroom environments. In the work by Li *et al.*,[58] a low-cost thermoplastic microfluidic probe was developed to perform mass spectrometry imaging on biological tissues. This technology maintained high spatial resolution comparable to glass probes while significantly reducing fabrication costs, enabling broader accessibility for biological research.

4 MFP integrations

Integrating additional physical modalities into the MFP technology can be achieved by incorporating thermal actuation, electric fields, dielectrophoretic (DEP) forces, electroporation, droplet microfluidics, or by combining MFPs with artificial intelligence and machine learning.[31,59] These integrations expand the application scope of MFPs, reduce system complexity, and support multiplexed experimentation. They offer significant advantages by minimizing time, effort, and material consumption.

4.1 Heat integration

By incorporating integrated heating elements, the MFP was transformed into a heat-assisted single-cell tweezer capable of precise thermal manipulation.[31] Adherent cell trypsinization is a common method for cell dissociation, typically requiring incubation at 37 °C. To perform single-cell dissociation, localized Joule heating can be utilized through heating elements embedded at the tip of the MFP in the form of pin-shaped electrodes.

4.2 Integration with mass spectrometry imaging

In another work by Liu *et al.*,[60] a microfluidic surface extractor (MSE) was designed and coupled with electrospray mass spectrometry to analyze the phospholipid content of different tumor cell types. Three types of cancer cell lines were investigated, and notable heterogeneity was observed among the cancer cells. The authors suggested that the designed MSE could have potential applications in the clinical analysis of cancer tissues. In the work by Li *et al.*, the integrated microfluidic probe (iMFP) was used to perform nano-DESI mass spectrometry imaging with comparable stability and sensitivity to capillary-based probes, achieving spatial resolution better than 25 μm and facilitating easier alignment and operation Fig. 5(a).[61] In their follow-up work with a high-resolution iMFP design, a spatial resolution of 8–10 μm and high throughput (scan rate 0.2 mm s^{-1}, completion in <29 min) was achieved without sacrificing sensitivity.[62] Similarly, Jiang *et al.* demonstrated a pneumatically assisted MFP that integrates external pressure modulation to enhance mass spectrometry imaging performance, improving extraction efficiency and image quality by stabilizing liquid interfaces during analysis.[63]

4.3 Electrical integration

Dielectrophoresis (DEP) is another phenomenon that involves electric fields to manipulate cells using their unique dielectric properties. When exposed to a non-uniform electric field, cells (which are dielectric by nature) develop a dipole moment and move towards or away from areas of higher field intensity based on their characteristics and the applied field frequency. In a recent study,[56] researchers developed the MeFP that integrates microelectrodes for DEP-based cell manipulation within an open, channel-less MFP system. The MeFP allows for sequential cell separation and patterning, utilizing DEP forces to selectively capture target cells Fig. 5(b). This technique enables dynamic control of cell co-culture patterns for cellular interaction studies. Subsequent

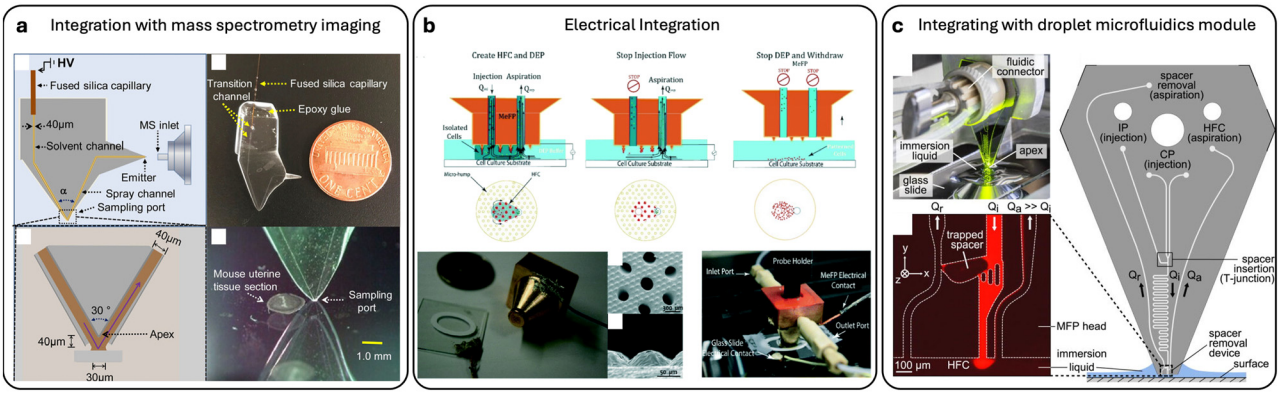

Fig. 5 MFP integrations. (a) Design and assembly of the integrated microfluidic probe for nano-DESI MSI, schematic drawing of the iMFP, an image of the iMFP, a schematic illustration of sampling port and liquid bridge between the probe and sample, and an image of the sampling port on top of a glass surface near a mouse uterine tissue sample. Reproduced from ref. 61 with permission from *Angewandte Chemie International Edition*, copyright 2020. (b) Schematics showing the working concept of the MeFP for sequential cell separation and patterning. Gold coated MeFP and ITO coated glass slide with electrical contacts, SEM images of (i) microfluidic apertures and (ii) side view of the hump-shaped electrodes. Reproduced from ref. 56 with permission from *Lab on a Chip*, copyright 2019. (c) Image showing a vertically mounted MFP head processing a surface on an inverted microscope, schematic of the MFP with inlets for injection of CP and IP liquids, as well as an on-chip spacer insertion junction and serpentine channel were used to test the spacer-removal module, and a micrograph of the immersed apex showing the spacer-removal module and hydrodynamic flow confinement. Reproduced from ref. 59 with permission from *Applied Physics Letters*, copyright 2015.

developments included a multiphysics MFP for single-cell manipulation and targeted drug delivery.[30] Further advancement was the developed NMP for genetic manipulation and analysis of single cells, combining electropermeabilization, hydrodynamic flow confinement, and contactless scanning. Macromolecules were precisely delivered into cells and single-cell nano-biopsies were performed.[31] The NMP consists of fluidic apertures and hump-shaped electrodes that confine reagents and electric signals with single-cell resolution. They successfully used the NMP to extract the cytoplasmic content of single PC3 and HeLa cells and evaluated the expression of a target gene.[64]

4.4 Integrating with droplet microfluidics module

The basic principle of MFP technology targets a single microscale sample at a given time. Since the MFP is mobile and can scan across substrates, it can target multiple samples sequentially. Therefore, MFP technology is generally considered a low-throughput method. Chemical samples, nanosamples, or products of reactions need to be delivered or collected separately to minimize crosstalk and sample mixing during sequential MFP processing. For example, in one study, sequential chemistry experiments were successfully performed using a specially designed MFP head. The MFP was designed to integrate a module that selectively removes immiscible spacers from the flow, allowing for precise and flexible chemical processing Fig. 5(c).[59] This MFP enables the handling of multistep chemical processes for a range of sequential liquid deliveries while preventing cross-contamination. In their work, oil spacers were used, and flow segmentation was accomplished by inserting immiscible-phase spacers between slugs of continuous-phase liquid to reduce dispersion. A 30% reduction in fluctuation of the confined liquid footprint was achieved using a three-channel module. The removal rate of immiscible spacers from an aqueous flow reached up to 15 spacers per second while maintaining HFC of the processing liquid.

4.5 Integration of structural features

Mesa structures were integrated in the work presented in ref. 29 to generate microvortices for enhanced fluid mixing and cell capture. The MFP design incorporated radially arranged herringbone (HB) features and was fabricated using stereolithography-based 3D printing. The resulting device, referred to as the HB-MFP, is simple, robust, and suitable for high-throughput sample processing. It also allows direct access to captured CTCs for downstream analysis. The system is channel-free and consists of two physically separated components: a bottom capture substrate and a top fluid delivery system. The HB-MFP was used to scan an open, biofunctionalized substrate and successfully capture CTCs from prostate cancer blood samples by targeting EpCAM, PSMA, and PSA antigens. Another work that presented mixing was the work by Luo *et al.*[65] They presented an open-space fluidic online mixing (OFM) system that enables region-specific control of membrane fusion by confining fluid flows through HFC to generate a localized acidic online mixing region. This system precisely triggered the fusion of small unilamellar vesicles (SUVs) and budded virions (BVs) into supported lipid bilayers (SLBs) in the micrometer scale area of single-cells, allowing fusion to be controlled *in situ*. Furthermore, the developed OFM system provided a versatile platform to monitor lipid lateral diffusion post-fusion holding potential for studying various vesicle–membrane interactions, intracellular compartment fusions, and single-cell membrane processes with high spatial precision.[65]

5 MFP biological applications

MFPs have transformed biological experimentation by enabling precise, localized interactions with tissues, cells, and subcellular environments. Their ability to deliver, extract, or manipulate fluids in open systems with high spatial and temporal resolution has opened new possibilities across biomedical research. From perfusing tissue slices and capturing CTCs to stimulating individual cells and enabling high-resolution biopatterning, MFPs offer unique advantages for real-time, dynamic, and non-destructive biological studies. The following applications illustrate how MFPs are being used to advance tissue diagnostics, single-cell analysis, molecular sampling, and spatial bioengineering.

5.1 Tissue processing

Biopsy-derived tissue slices are commonly analyzed using laboratory techniques such as histopathology, which assesses cellular morphology for pathological changes, and immunohistochemistry (IHC), which employs antibody-based detection of disease-associated proteins, including cancer biomarkers.[66,67] Additional analytical approaches include molecular diagnostics, flow cytometry, and microarray profiling. While these methods yield valuable insights, they often lack the spatial specificity and molecular sensitivity required for single-cell or subcellular analysis. Closed microfluidic systems have been utilized for tissue slice studies in contexts such as electrophysiological monitoring, biomarker profiling, and toxicological assessments.[68,69] However, these enclosed systems are limited by geometric constraints, technical complexity, and restricted mass transport. In addition, materials such as PDMS may absorb or leach uncrosslinked compounds (drugs or oligomers), introducing variability in drug dosing and potential cytotoxicity. In contrast, open microfluidic systems overcome these limitations by enabling localized perfusion, real-time imaging, and analysis at single-cell resolution. MFP platforms, in particular, offer spatiotemporal control *via* HFC and scanning capabilities, facilitating precise and minimally invasive examination of tissue samples. These platforms improve detection sensitivity, reduce antibody cross-reactivity, and preserve the native architecture of tissue slices, thereby enhancing physiological relevance.[45] As a result, a range of MFP-based approaches has emerged for the high-resolution analysis of biopsy specimens and animal-derived tissue sections.

The use of the MFP to locally perfuse tissue slices cultured using conventional methods, such as the roller-tube technique, is demonstrated in Fig. 6(a). A perfusion chamber was designed to fit in an inverted confocal microscope for high magnification imaging, and a red fluorescent dye was used to map its distribution in 3D within the slice.[45] While the produced HFC confines reagents at the tissue surface, their subsequent movement inside the tissue is governed primarily by diffusion, leading to depth-dependent penetration, slower reagent equilibration in deeper layers, and spatial variability dictated by the local extracellular matrix architecture.[45] The MFP was fabricated using soft lithography and made of PDMS, featuring six micrometer-scale apertures that can be used for injection and aspiration

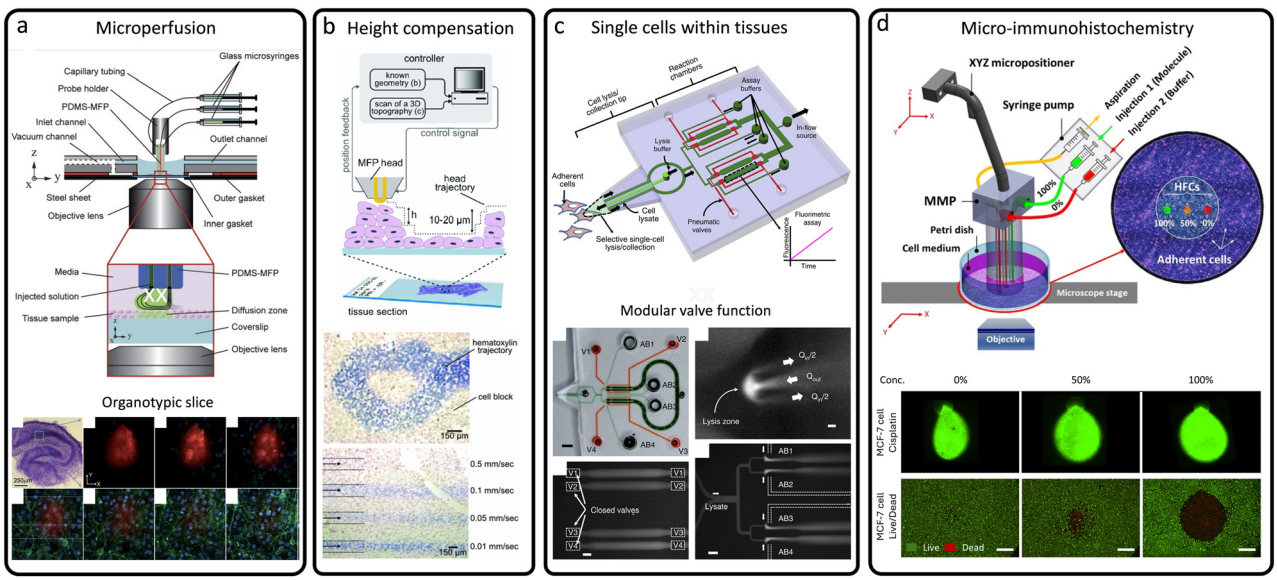

Fig. 6 Tissue-level applications of MFPs. (a) Perfusion chamber and PDMS-based MFP used for microperfusion of organotypic brain slices. Reproduced from ref. 45 with permission from *Lab on a Chip*, copyright 2010. (b) cMFP as an advanced and versatile MFP for local processing of tissue sections and biological specimens with a height-compensation mechanism. Reproduced from ref. 70 with permission from *Review of Scientific Instruments*, copyright 2014. (c) MFP applied to single-cell biochemical analysis within adherent tissue culture. Reproduced from ref. 71 with permission from *Nature Communications*, copyright 2014. (d) Microfluidic mixing probe (MMP) enabling the generation of multiple concentration-varying flow dipoles across a confluent cell culture in a Petri dish. Reproduced from ref. 73 with permission from *Scientific Reports*, copyright 2025.

of solutions. The MFP was successfully used to perfuse a small number of cells in a brain slice while concurrently imaging the perfused dye and subcellular structures using confocal fluorescence microscopy.[45] A similar MFP technology was further optimized with a height-compensation mechanism,[70] allowing the MFP, termed cMFP, to follow non-planar surfaces in tissue and cellular ensembles, making it suitable for hovering over morphologically changing breast cancer tissue slices, as shown in Fig. 6(b). Building on these advances, Sarkar *et al.* developed an MFP designed for biochemical analysis at the single-cell level,[71] enabling precise, non-destructive analysis of single adherent cells in their native culture context. Similarly, Mao *et al.* developed an open-space MFP platform to quantify single-cell adhesion of circulating tumor cells on endothelial layers, enabling real-time detachment assays that uncover heterogeneity in adhesion strength and drug response.[72]

Unlike conventional single-cell methods that require dissociation and isolation, which disrupt the cellular environment and spatial information, this MFP selectively lyses individual adherent cells and aspirates their contents for downstream analysis, as shown in Fig. 6(c). The platform was applied to human hepatocellular carcinoma cells to measure kinase activity and housekeeping protein levels, either independently or in parallel from single cells. This approach provides critical insights into how heterogeneous cells process signals *in situ*, linking local microenvironments to intracellular biochemical responses. Ali *et al.* developed a 3D-printed microfluidic mixing probe (MMP) that enables multiplexed gradient generation atop a confluent cell culture.[73] The MMP integrates an internal pre-mixer and a linear array of injection and aspiration apertures, allowing simultaneous formation of discrete concentration gradients within an open microfluidic environment. This design solves the challenge of localized dose variation across cell cultures or tissue slices, enabling controlled, contamination-free exposure to chemotherapeutic agents, as shown in Fig. 6(d). By facilitating spatially resolved drug screening, the MMP offers a powerful tool for personalized medicine and quantitative pharmacological studies. Shiku *et al.* demonstrated an MFP-based dual-capillary system that locally lysed adherent cells and spheroids, enabling direct collection of mRNA for downstream genetic analysis.[74]

Horayama *et al.*[75] developed an MFP device that enables precise, localized chemical stimulation for cell-based assays. The device features MFP channels embedded along the walls of cell culture microchannels, allowing control of the stimulation area from the scale of a single cell to a small group of cells.[75] The platform was experimentally validated through localized cell staining and selective cell collection as shown in Fig. 7(a), demonstrating its utility for probing cell–cell interactions and enabling spatially targeted single-cell analysis. Lovchik *et al.*[76] also introduced a new staining method called micro-IHC, which allows for staining tissue sections at the microscale as shown in Fig. 7(b). The method used a vertical microfluidic probe (vMFP) design to confine nanolitres of antibody solutions over micrometre-sized areas of tissue sections.[76] The vMFP operates above the tissue section, allowing for interactive positioning and even staining of individual cores of tissue microarrays with multiple antigens. The authors suggested that this method is preservative toward tissue samples and reagents, alleviates antibody cross-reactivity issues, and allows for a wide range of staining conditions to be applied to a single tissue section. In a follow-up work,[77] they introduced an approach for rapid, localized IHC staining of tissue sections using an MFP with

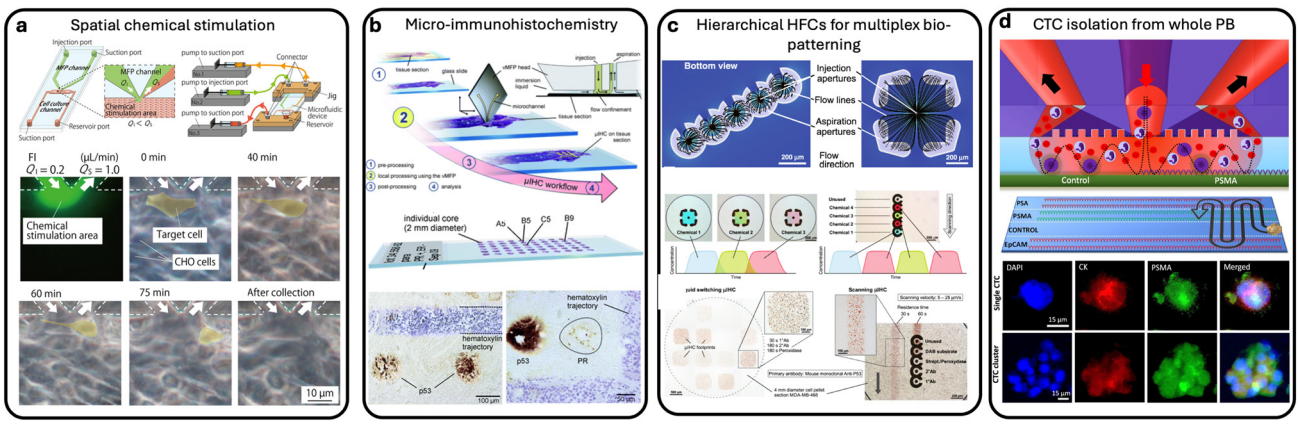

Fig. 7 Applications of MFPS for cell analysis within tissues. (a) MFP-integrated device enabling spatially controlled chemical stimulation in cell-based assay. Reproduced from ref. 75 with permission from PLoS One, copyright 2016. (b) Concept and workflow of μIHC using a vMFP. Dewaxing and rehydration of the tissue are performed according to conventional IHC. Reproduced from ref. 76 with permission from *Lab on a Chip*, copyright 2012. (c) Experimental results of two implementations of sequential chemistry used to complete the full μIHC protocol on formalin-fixed paraffin-embedded cell blocks. Reproduced from ref. 77 with permission from *Microsystems and Nanoengineering*, copyright 2020. (d) HB-MFP for multiplexed affinity-capture of prostate circulating tumor cells. Reproduced from ref. 29 with permission from *Advanced Materials Technologies*, copyright 2021.

geometrically optimized apertures. This system enables precise spatial confinement of biochemical reagents over circular or square footprints on the tissue surface, as shown in Fig. 7(c). By delivering a time-optimized sequence of reagents directly to the tissue, the MFP significantly reduces the duration of key IHC incubation steps to under 30 minutes, substantially faster than conventional protocols, which typically require over an hour. This method addresses the need for accelerated and localized tissue biomarker analysis, making it particularly valuable for intraoperative diagnostics, where rapid feedback is critical. Building on this, the same authors described in a recent work the use of this tool to develop a quantitative micro-IHC approach that captures the dynamic evolution of the staining signal, allowing for precise assessment of antigen density and improved stratification of breast cancer samples.[78]

Li *et al.* optimized the design of an MFP, named ionization microfluidic probe (iMFP), which allows for high-throughput imaging of tissue sections. By increasing the dimensions of the primary and spray channels and optimizing the spray voltage and solvent flow rate, stable operation of the iMFP at low and high scan rates was achieved. The iMFP produced high-quality images of mouse uterine and brain tissue sections in significantly less time than previous designs, allowing for a 10- to 15-fold increase in experimental throughput.[79] Furthermore, in a special consideration of whole blood as a tissue sample bearing heterogeneity in its cell content, MFPs were also used to analyze, in a clinical study, whole blood from cancer patients, in particular, the HB-MFP, which was discussed in previous sections. The HB-MFP demonstrated efficient capture of CTCs from prostate cancer blood samples based on their specific antigen expressions, as shown in Fig. 7(d). The system can capture CTCs in a single run, even clusters of up to 40–50 cells.[29] The number of CTCs captured ranged from 6 cells per mL in localized cancer patients to up to 280 cells per mL in metastatic cancer patients. Multiplex profiling of

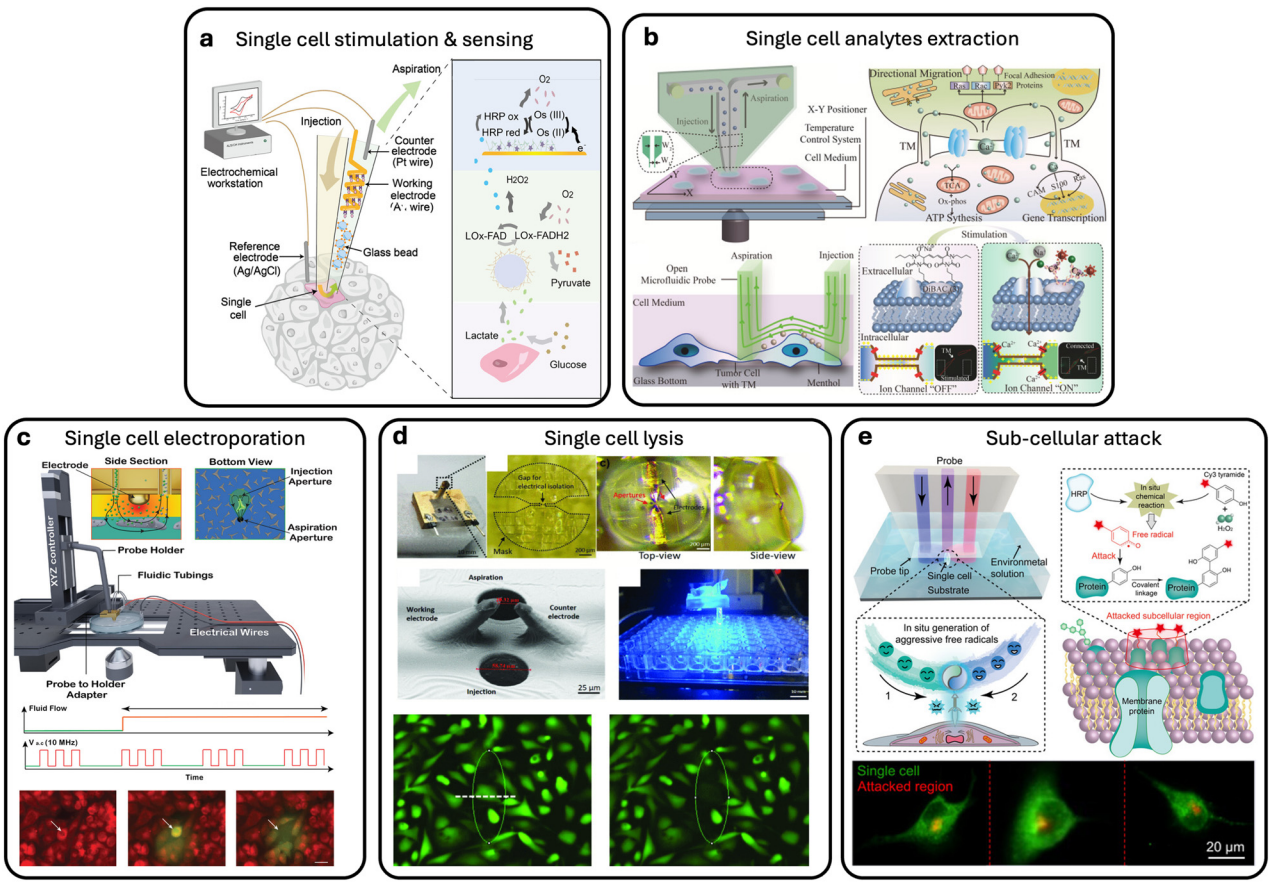

Fig. 8 Applications of MFPs for single cell analysis. (a) MFP developed for localized perfusion, *in situ* single-cell stimulation, and real-time electrochemical detection of lactate response. Reproduced from ref. 82 with permission from *Analytical Chemistry*, copyright 2021. (b) MFP developed for *in situ* monitoring of calcium signaling through tumor microtubes enabling analysis of single cell–cell communication. Reproduced from ref. 80 with permission from *Biosensors and Bioelectronics*, copyright 2022. (c) MFP developed for spatiotemporally resolved single-cell electroporation and analyses. Reproduced from ref. 31 with permission from *Small*, copyright 2021. (d) Integrated MFP developed for single cell cytoplasmic biopsy and analysis. Reproduced from ref. 64 with permission from IEEE, copyright 2022. (e) MFP developed for *in situ* stable generation of reactive intermediates for subcellular free radical attack and membrane labelling. Reproduced from ref. 81, with permission from *Angewandte Chemie International Edition*, copyright 2021.

CTCs revealed cellular phenotypes based on PSMA and PSA expression levels.

5.2 Cellular and subcellular processing

The native cellular microenvironment is composed of various elements including the extracellular matrix, soluble molecules, and neighbouring cells. Stimuli and responses in microenvironments vary widely in timescale, from over a day such as in circadian rhythms to milliseconds as in electrical impulses. Conventional cell cultures manage environments for cell populations on the scale of minutes but lack the resolution to address individual cells in shorter time frames. Microfluidic technologies provide greater spatiotemporal control, allowing for rapid experimental processes that enable solution exchange at the scale of milliseconds. MFPs' scanning capacity, high spatial control, and low shear stress make them well suited for single-cell analysis, and in applications that exploit tightly confined flow zones, they can also reduce reagent usage compared to traditional bulk-flow approaches. Applications of MFPs for single-cell studies include the selective detachment and collection of individual cells, detection of secreted biomolecules from single cells,[80] cytoplasm extraction,[33] membrane labelling,[81] and precise stimulation or induction of cells.[82]

The earliest work of an MFP[13] demonstrated for the first time the selective detachment and collection of a single adherent living cell using an MFP. By confining a microjet of trypsin (a proteolytic enzyme commonly used in bulk cell harvesting) within a precisely controlled local flow field, the MFP enabled spatially targeted enzymatic treatment at single-cell resolution. This approach allowed for the detachment of an individual fibroblast cell from a monolayer culture without affecting neighboring cells or disrupting the surrounding microenvironment. The localized delivery ensured that trypsinization remained confined to the targeted cell, preserving the viability and adhesion of adjacent cells even after prolonged operation.

In more recent reports, Zhou *et al.* described an MFP-based platform for real-time, noninvasive electrochemical monitoring of single-cell metabolism, enabling the detection of lactate secretion in response to glucose stimulation,[82] as shown Fig. 8(a). By integrating continuous localized perfusion with downstream enzymatic decomposition and electrochemical sensing, the system provides precise spatial resolution at the single-cell level. This platform addresses the challenge of capturing dynamic metabolic responses from individual cells within heterogeneous populations, offering a valuable tool for the study of cellular microenvironment interactions. In a related approach, Song *et al.* developed an MFP that is capable of chemically perforating the plasma membrane to deliver proteins into single cells with high spatial precision, enabling localized intracellular delivery for probing cell function and manipulating individual cell responses.[83] In another work by Bondarenko *et al.*, an electrochemical push–pull MFP was developed that integrates microfluidics with electrochemical processing.[84] This device enabled precise delivery of chemical compounds to targeted areas. It was used for spatiotemporal cell perturbation, enabling electrochemical targeting of a few cells and fluidic delivery to hundreds, as demonstrated through both simulations and experiments. The MFP supports dynamic and reversible cell perturbation, making it valuable for studying the effects of pH on cancer cell growth and for analyzing extracellular samples.

In the work by Feng *et al.*, the MFP was used to investigate dynamic calcium signal transmission between single cells connected by tumour microtubes, as shown in Fig. 8(b). The MFP provided single cell stimulation with low cellular damage *via* a minimally invasive HFC, eliminating the complicated process for the capture of single cell pairs. The MFP also enabled a different stimulation environment for the target cell pair, allowing the exploration of the heterogeneity in depolarization response in glioma cells.[80] Another advancement is the NMP, which was developed to perform multiple manipulation procedures on living single cells within their physiological tissue environment, as shown in Fig. 8(c).[31] The technology's adjustable spatial capability was demonstrated by transfecting adjacent single cells with different DNA plasmid vectors. The NMP also enables controllable cytoplasm extraction from living single cells. In a follow-up study, Sofela *et al.* developed an integrated MFP, as shown in Fig. 8(d). This tool enables minimally invasive cytoplasmic biopsy of single adherent cells while preserving their spatiotemporal integrity, a critical factor for accurate omics analysis.[64] The MFP design combines electro-permeabilization for transient membrane-poration with HFC for localized extraction of intracellular material.

In the work by Song *et al.*,[85] the MFP was used to precisely induce plasma membrane injury in single cells using HFC. The device enabled controlled exposure to digitonin and real-time tracking of membrane repair *via* fluorescence imaging. It revealed how factors like calcium, magnesium, and glucose affect repair, highlighting variability between cells. This approach offers a versatile tool for studying single-cell injury and recovery.

In cellular applications, a special form of the MFP was introduced by Mao *et al.*,[86] which is the micro-chemical pen (MCP). It enables region-selective surface modification by performing multi-reagent reactions directly on solid substrates in open solutions. Unlike conventional MFPs that confine single flows, the MCP exploits laminar streams and diffusion layers to achieve tunable working regions from 4.5–100 μm. It has been applied to polymer patterning, silver electrode fabrication, and selective biofilm modification, all while maintaining low shear stress compatible with live cells. Thus, the MCP expands the application range of MFPs from controlled fluid delivery to true microscale chemical patterning. In another work by Mao *et al.*,[72] the authors found that single circulating tumor cells (CTCs) could be analyzed on endothelial cell layers using an open microfluidic platform. They showed that this method allowed

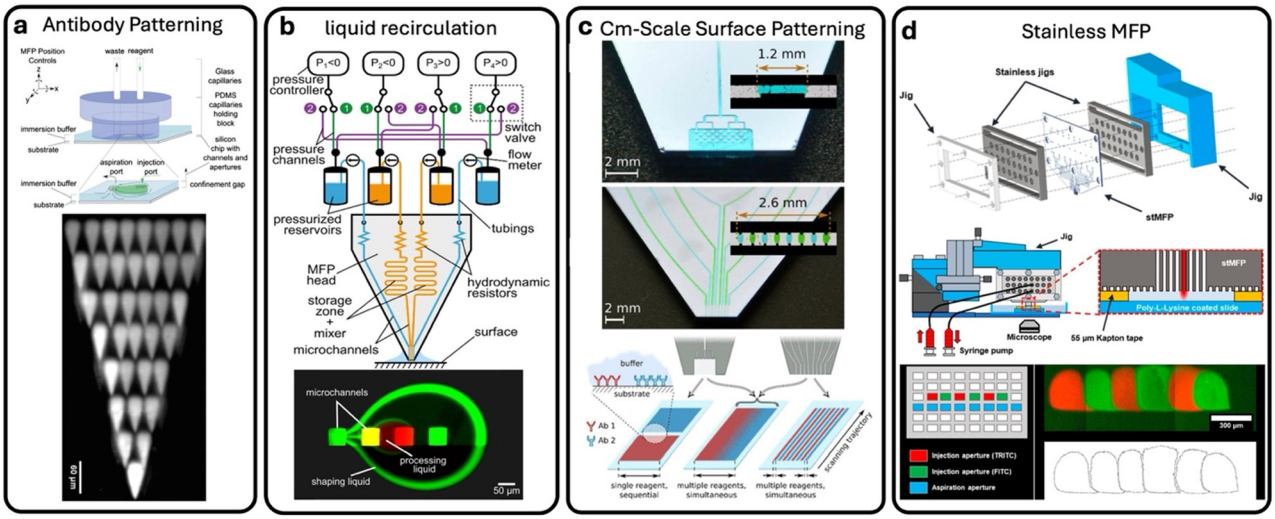

Fig. 9 Applications of MFPs for bio-patterning. (a) Patterning of fluorescein-labeled biotin on a streptavidin-coated epoxy slide. The patterns were formed by rapidly moving the MFP from spot to spot, using injection and aspiration flow rates of 1 and 10 nL s^{-1}, respectively. Reproduced from ref. 87, with permission from *Review of Scientific Instruments*, copyright 2010. (b) Hierarchical MFP developed for multiplex biopatterning. Reproduced from ref. 48 with permission from *Langmuir*, copyright 2014. (c) Strategies for interacting with immersed substrates on the centimeter-scale using hydrodynamic flow confinement. Reproduced from ref. 91 with permission from *Langmuir*, copyright 2016. (d) Stainless-steel MFP developed for precise use of reagents. Reproduced from ref. 57 with permission from *AIP Advances*, copyright 2021.

non-destructive, high-resolution measurement of adhesion strength at the single-cell level. The study revealed that different CTC types exhibit variable adhesion and that drug treatments, such as temozolomide, can reduce adhesion strength. This approach offers a promising strategy for cancer drug screening and understanding tumor metastasis mechanisms.

MFPs further pushed the processing resolution towards subcellular components. Zhang *et al.* developed an MFP that generated and confined free radicals to a microregion for stable subcellular stimulation.[81] By optimizing the chemical reaction, reactive radicals were directed to attack the desired subcellular region of a single cell. They also synthesized fluorescent tyramide free radicals that covalently bound with membrane proteins to stain the target microregion of a single cell as, shown in Fig. 8(e). The method enables stimulation with short-lived reactive intermediates at the single-cell or subcellular level and allows for selective membrane labeling.

5.3 Bio-patterning and molecular analysis

Surface bio-patterning is a common practice relevant to various research fields. While microfluidic networks and microcontact printing address some challenges of the traditional protocols (*e.g.* microplotting), the MFP combines the advantages of both microfluidics and microplotting, enabling precise and flexible protein patterning. The MFP can process large surfaces by scanning across them, making it particularly suitable for protein micro-arraying,[87] as shown in Fig. 9(a). Additional applications of the MFP include gradient formation, laminar-flow patterning, microscale and molecular erasing, and localized cell staining.[13,88]

In recent work, researchers refined a previously developed hHFC configuration[48] to make bio-patterning more efficient and precise. The work utilized the hHFC concept to improve reagent utilization in bio-patterning applications, reducing dilution, and allowing solution recirculation within the MFP,[88,89] as shown in Fig. 9(b). Furthermore, hHFCs provide the advantage of fast switching between processing liquids and precise control of surface reaction kinetics. For instance, they were used to simultaneously deposit two or more analytes on adjacent areas of the same surface for multiplexed analysis of individual cores of a tissue microarray.[77,90] In another work, an MFP device was developed for spatially defined, multiplexed bio-patterning on immersed substrates at the centimeter scale.[91] This platform utilizes HFC to localize submicroliter reagent volumes on targeted surface regions, enabling both sequential and simultaneous delivery of multiple biochemical agents, as shown in Fig. 9(c). The system supports the creation of chemical gradients and high-resolution patterns, facilitated by non-contact scanning and convection-enhanced reaction kinetics. This approach addresses key limitations related to multiplexing and scalability in bio-patterning.

To regulate spatial diffusion of fluorescent molecules, a 3D-integrated MFP device with vertically oriented microchannels was developed.[92] The MFP was utilized to alter the physiological response of cells within a restricted area by altering the local and temporal concentrations of biomolecules such as ATP. Instead of depositing reagents, MFPs can also be used to retrieve biomolecules. The MFP has also been reported to be used in subtractive patterning. For instance, the MFP was used as a "fluidic biomill".[93] To demonstrate the utility of this method, a biotin functionalized biochip was fabricated from a polystyrene

slide and its functionalities were validated by implementing on-chip electrokinetic sample focusing, pressure driven flow, and a surface-based reaction. Another work demonstrated high-resolution, large-area biopatterning *via* the densely packed 2D aperture array of the stMFP.[57] The device enabled precise, tunable biopatterning, demonstrated through fluorescent antibody deposition across treatment areas ranging from 3.3×10^3 μm^2 to 4.5×10^5 μm^2, depending on the aperture configuration, as shown in Fig. 9(d). It also allowed the simultaneous formation of multiple discrete biopatterns using different reagents, as shown by alternating injections of two antibodies to generate six independent treatment zones.

MFPs have advanced biopatterning by enabling precise, multiplexed, and non-contact reagent delivery using HFC. Indeed, innovations like hHFC and 3D-integrated designs have improved reaction control, spatial resolution, and reagent efficiency. Subtractive techniques and cell manipulation further expanded their utility. However, challenges remain in fully automating probe alignment and maintaining stability over curved or irregular surfaces. One possible solution is to integrate MFP technology with adaptive control systems and artificial intelligence (AI) for *in situ* feedback control.

5.4 MFP as a fabrication tool

In addition to their applications in cell-manipulation and biopatterning, MFP-like devices have recently emerged as precise tools for fabricating nanowires with exceptional sensitivity for biosensing applications, leveraging their unique HFC capabilities to pattern materials with high spatial resolution. In the work by Lin *et al.*,[94] an HFC-based microfluidic pen was utilized to fabricate localized nanowires for ultrasensitive protein detection. The technique enabled direct deposition of nanowires on target surfaces by confining reactive flows within micrometer-scale regions. This approach achieved impressive detection limits down to 0.089 fg mL^{-1} for immunoglobulins (IgA and IgG), demonstrating a major sensitivity improvement over conventional fabrication method. These developments were built on their prior work.[95] They showed a regioselective fabrication method using the pen system, allowing for the controlled growth of gold nanowires.[95] Their strategy achieved attomolar-level detection sensitivity (1 aM) for target proteins, showcasing the extreme precision and versatility of MFP-based flow confinement in localized material patterning under ambient conditions.[96] Collectively, these studies highlight the capability of the MFP and pen technologies to serve as high-precision fabrication tools for nanowires, opening new pathways for constructing ultra-sensitive, miniaturized biosensors through localized material deposition.

6 Discussion and conclusion

This review provides a comprehensive overview of MFPs as versatile open microfluidic systems, focusing on their operational principles, engineering advancements, and applications in biomedical sciences. We begin by outlining the foundational fluidic principles of MFPs, including the concept of HFC, which enables non-contact, localized delivery and aspiration of reagents. This capability is critical for single-cell and subcellular manipulation. We also discuss the fluidic dynamics underlying HFC formation, including the influence of flow rate ratios, aperture geometry, and shear stress on interaction resolution. The chronological development of MFP microfabrication strategies is presented, highlighting the shift from planar microstructures to more complex, three-dimensional designs incorporating soft lithography, 3D printing, thermal bonding, and stainless-steel stacking. Further integrations such as electropermeabilization, thermal actuation, and droplet-based compartmentalization are also discussed, emphasizing their role in expanding the functional scope of MFPs. Applications are categorized across spatial scales, from intracellular biopsies and cell detachment to tissue-level staining and biopatterning. Particularly notable are recent innovations such as hHFCs for improved reagent utilization and stMFPs for enabling large-area, high-resolution multiplexed biopatterning.

6.1 MFP limitations

MFP technology is an emerging platform with significant potential in precision bioprocessing and spatially resolved analysis. Although widely used in research laboratories, current implementations still face several system-level and engineering limitations that must be addressed to support broader scalability and integration into routine biomedical workflows. One recurring technical challenge is the susceptibility of small apertures to blockage by debris, air bubbles, or surface irregularities, which can affect flow stability and compromise reagent confinement. Similarly, precise control of the probe–surface gap remains essential for consistent performance. Variations in sample topography or mechanical drift can influence liquid contact and assay uniformity, and although feedback mechanisms such as gas-bubble-based pressure sensing have been introduced, these often require additional calibration or instrumentation that complicates integration into compact platforms.

Advances in automation and scalability are still needed. Current MFP platforms are predominantly designed for benchtop research environments, and fully integrated systems with automated alignment, scanning, and real-time feedback remain limited. Enhancing compatibility with robotic stages, closed-loop control systems, and modular interfaces is therefore an important direction for future development. Material constraints also play a role: despite progress enabled by 3D printing and micromachining, available materials still impose limits on biocompatibility, chemical resistance, and optical characteristics, which in turn restrict the range of biological assays that can be conducted. Addressing these challenges will require

continued innovation in microsystem design, materials engineering, and system integration to improve robustness, reproducibility, and overall platform maturity.

6.2 Outlook and future work

The MFP technology is progressing toward becoming a versatile "lab-on-a-tip", capable of precise, on-demand processing, patterning, and sampling across cellular and tissue scales. Future developments should focus on enhancing performance, modularity, and platform standardization to increase accessibility and expand adoption in both research and clinical environments. Standardizing operational modules and workflows represents an important step in this direction, and early efforts have already demonstrated the feasibility of such approaches. Additional opportunities lie in integrating thermal, acoustic, optical, or electrokinetic functionalities to actively manipulate cells and biomolecules, enabling expanded capabilities such as programmable sorting, trapping, and stimulation.

Improvements in microfabrication, including high-resolution 3D printing and two-photon polymerization, are expected to support the construction of increasingly complex probe architectures incorporating sensors and multi-material components. Moreover, a key direction is the modularization and standardization of all MFP operations to improve accessibility. Initial efforts in this direction have been demonstrated in a recent study.[97] Furthermore, combining MFPs with adaptive and closed-loop control systems powered by real-time imaging and AI-based feedback could enable autonomous operation over heterogeneous or non-planar samples, thereby improving precision and reproducibility. From a translational perspective, MFPs hold strong promise for point-of-care diagnostics, intraoperative tissue analysis, and spatial omics by enabling localized and multiplexed assays with minimal sample preprocessing. Continued efforts toward device standardization, integration, and regulatory alignment will be essential for realizing their full impact in clinical and high-throughput settings.

6.3 Conclusion

In summary, MFPs are poised to play a transformative role in biomedical research, diagnostics, and therapeutic monitoring. Their ability to deliver, extract, and pattern fluids with high spatial and temporal precision has opened new possibilities across biological scales, from intracellular analysis to tissue-level processing. The technology has already demonstrated unique advantages in applications such as localized single-cell stimulation, subcellular biopsies, high-resolution biopatterning, and spatially resolved omics. However, realizing the full potential of MFPs requires continued innovation across several fronts. Advances in fluidic actuation and materials will improve performance and compatibility with diverse biological environments. Progress in fabrication techniques, including high-resolution 3D printing and hybrid lithography, will enable more complex and customizable probe architectures. System-level automation and closed-loop feedback integration will be key to enhancing reproducibility and enabling operation over irregular surfaces and dynamic samples. Functional integration with optical, thermal, acoustic, and electrical modules will expand MFP utility for multimodal analysis and precision manipulation of biological targets. Clinically, MFPs are well positioned to address critical challenges in point-of-care diagnostics, intraoperative decision-making, and spatial biology, offering minimally invasive tools for localized and multiplexed assays. Moving forward, the convergence of MFP technology with AI-driven feedback, robotics, and standardized modular components will be essential for translating this powerful platform from benchtop research to routine biomedical and clinical workflows.

Author contributions

D. S. A. and A. G. contributed to the formal analysis, visualization, and writing of the original draft, as well as to the review and editing of the manuscript, while D. S. A. and M. A. Q. contributed to the conceptualization of the study; M. A. Q. also led the supervision, funding acquisition, and project administration. All authors contributed to the interpretation of the results and approved the final version of the manuscript.

Conflicts of interest

There are no conflicts to declare.

Data availability

No primary research results, software, or code have been included, and no new data were generated or analysed as part of this review.

Acknowledgements

Dima Samer Ali acknowledges support from the NYUAD Global PhD Fellowship. The authors gratefully acknowledge financial support from New York University Abu Dhabi (NYUAD) and the technical support provided by the Core Technology Platforms (CTP) at NYUAD.

References

1 G. M. Whitesides, The origins and the future of microfluidics, *Nature*, 2006, **442**(7101), 368–373.
2 A. Manz, *et al.*, Planar chips technology for miniaturization and integration of separation techniques into monitoring systems: Capillary electrophoresis on a chip, *J. Chromatogr. A*, 1992, **593**(1–2), 253–258.
3 P. S. Dittrich and A. Manz, Lab-on-a-chip: microfluidics in drug discovery, *Nat. Rev. Drug Discovery*, 2006, **5**(3), 210–218.
4 C. L. Hansen, *et al.*, A robust and scalable microfluidic metering method that allows protein crystal growth by free

interface diffusion, *Proc. Natl. Acad. Sci. U. S. A.*, 2002, **99**(26), 16531–16536.
5 B. Zheng, *et al.*, A droplet-based, composite PDMS/glass capillary microfluidic system for evaluating protein crystallization conditions by microbatch and vapor-diffusion methods with on-chip X-ray diffraction, *Angew. Chem., Int. Ed.*, 2004, **43**(19), 2508–2511.
6 A. R. Wheeler, *et al.*, Microfluidic device for single-cell analysis, *Anal. Chem.*, 2003, **75**(14), 3581–3586.
7 P. S. Dittrich and A. Manz, Single-molecule fluorescence detection in microfluidic channels—the Holy Grail in μTAS?, *Anal. Bioanal. Chem.*, 2005, **382**, 1771–1782.
8 P.-A. Auroux, *et al.*, Miniaturised nucleic acid analysis, *Lab Chip*, 2004, **4**(6), 534–546.
9 D. N. Breslauer, P. J. Lee and L. P. Lee, Microfluidics-based systems biology, *Mol. BioSyst.*, 2006, **2**(2), 97–112.
10 D. Huh, *et al.*, Microfluidics for flow cytometric analysis of cells and particles, *Physiol. Meas.*, 2005, **26**(3), R73.
11 R. Suh, S. Takayama and G. D. Smith, Microfluidic applications for andrology, *J. Androl.*, 2005, **26**(6), 664–670, DOI: 10.2164/jandrol.05119.
12 C.-H. Hsu, C. Chen and A. Folch, "Microcanals" for micropipette access to single cells in microfluidic environments, *Lab Chip*, 2004, **4**(5), 420–424.
13 D. Juncker, H. Schmid and A. E. Delamarche, Multipurpose microfluidic probe, *Nat. Mater.*, 2005, **4**(8), 622–628, DOI: 10.1038/nmat1435.
14 M. A. Qasaimeh, T. Gervais and D. Juncker, Microfluidic quadrupole and floating concentration gradient, *Nat. Commun.*, 2011, **2**(1), 464.
15 G. V. Kaigala, *et al.*, A vertical microfluidic probe, *Langmuir*, 2011, **27**(9), 5686–5693.
16 A. Brimmo, P. A. Goyette, R. alnemari, T. Gervais and M. Qasaimeh, 3D Printed Microfluidic Probes, *Sci. Rep.*, 2018, **8**(1), DOI: 10.1038/s41598-018-29304-x.
17 M. A. Qasaimeh, S. B. G. Ricoult and A. D. Juncker, Microfluidic probes for use in life sciences and medicine, *Lab Chip*, 2013, **13**(40), 40–50.
18 A. T. Brimmo and M. A. Qasaimeh, Microfluidic probes and quadrupoles: A new era of open microfluidics, *IEEE Nanotechnol Mag*, 2017, vol. 11, 1, pp. 20–31.
19 G. V. Kaigala, R. D. Lovchik and E. Delamarche, Microfluidics in the "Open Space" for Performing Localized Chemistry on Biological Interfaces, *Angew. Chem., Int. Ed.*, 2012, **51**(45), 11224–11240.
20 Q. Zhang, *et al.*, Emerging open microfluidics for cell manipulation, *Chem. Soc. Rev.*, 2021, **50**(9), 5333–5348.
21 A. Oskooei and G. V. Kaigala, Deep-Reaching Hydrodynamic Flow Confinement: Micrometer-Scale Liquid Localization for Open Substrates With Topographical Variations, *IEEE Trans. Biomed. Eng.*, 2017, **64**(6), 1261.
22 A. Ainla, G. Jeffries and A. Jesorka, Hydrodynamic Flow Confinement Technology in Microfluidic Perfusion Devices, *Micromachines*, 2012, **3**(2), 442–461, DOI: 10.3390/mi3020442.
23 M. Hitzbleck, *et al.*, The floating microfluidic probe: Distance control between probe and sample using hydrodynamic levitation, *Appl. Phys. Lett.*, 2014, **104**(26), 263501, DOI: 10.1063/1.4886117.
24 M. Safavieh, *et al.*, Two-Aperture Microfluidic Probes as Flow Dipoles: Theory and Applications, *Sci. Rep.*, 2015, **5**, 14885–14885.
25 E. Delamarche and G. V. Kaigala, *Open-space microfluidics*, Wiley, 2018.
26 A. Glia, P. Sukumar, A. T. Brimmo, M. Deliorman and M. A. Qasaimeh, Immuno-capture of cells in open microfluidics: microfluidic probes integrated with herringbone micro-mixers, *In Microfluidics, BioMEMS, and Medical Microsystems XVII*, SPIE, 2019, vol. 10875, pp. 207–213.
27 K. V. Christ and K. T. Turner, Design of hydrodynamically confined microfluidics: controlling flow envelope and pressure, *Lab Chip*, 2011, **11**(8), 1491–1491.
28 P. Choongbae, V. C. Kevin and T. T. Kevin, *Open Space Microfluidics*, 2018, pp. 47–61.
29 A. Glia, *et al.*, Herringbone Microfluidic Probe for Multiplexed Affinity-Capture of Prostate Circulating Tumor Cells, *Adv. Mater. Technol.*, 2021, **6**(6), 2100053.
30 A. Brimmo and M. A. Qasaimeh, *2020 International Conference on Manipulation, Automation and Robotics at Small Scales (MARSS)*, IEEE, 2020.
31 A. T. Brimmo, *et al.*, Noncontact Multiphysics Probe for Spatiotemporal Resolved Single-Cell Manipulation and Analyses, *Small*, 2021, **17**(24), 2100801.
32 A. Brimmo, A. Glia, P. Sukumar, R. Alnemari, A. Menachery, M. Deliorman and M. A. Qasaimeh, Integrated microfluidic probes for cell manipulation and analysis, *Proc. SPIE 10875, Microfluidics, BioMEMS, and Medical Microsystems XVII*, 2019, vol. 108750R, DOI: 10.1117/12.2515270.
33 M. Proulx, *et al.*, Open-space microfluidics as a tool to study signaling dynamics, *Lab Chip*, 2025, **25**(21), 5592–5605.
34 M. Safavieh, *MicroTAS*, 2010.
35 L. Bergeron-Sandoval, *et al.*, GTPase-dependent mechanointegration of shear-mediated cell contractility through dynamic binding of FLNa and FilGAP, *Front. Phys.*, 2022, **10**, 890865.
36 J. A. Espina, *et al.*, Response of cells and tissues to shear stress, *J. Cell Sci.*, 2023, **136**(18), DOI: 10.1242/jcs.260985.
37 M. J. Mitchell and M. R. King, Computational and experimental models of cancer cell response to fluid shear stress, *Front. Oncol.*, 2013, **3**, 44.
38 D. E. Brooks, The biorheology of tumor cells, *Biorheology*, 1984, **21**(1–2), 85–91.
39 H. Bruus, Governing equations in microfluidics, *Lab Chip*, 2014, **2011**(11), 3742–3751.
40 S. S. Rao, *The Finite Element Method in Engineering*, 2018.
41 H. S. Hele-Shaw, On the motion of a viscous fluid between two parallel plates, *Nature*, 1898, **58**(1489), 34–36.
42 E. Boulais and T. Gervais, The 2D microfluidics cookbook - modeling convection and diffusion in plane flow devices, *Lab Chip*, 2023, **23**(8), 1967–1980.
43 P. G. Drazin and N. Riley, *The Navier-Stokes equations: a classification of flows and exact solutions*, 2006.
44 H. Bruus, *Theoretical microfluidics*, Oxford university press, 2007, vol. 18.

45 A. Queval, *et al.*, Chamber and microfluidic probe for microperfusion of organotypic brain slices, *Lab Chip*, 2010, **10**(3), 326–334.
46 P.-A. Goyette, *et al.*, Microfluidic multipoles theory and applications, *Nat. Commun.*, 2019, **10**(1), 1781.
47 P.-A. Goyette, É. Boulais, M. Tremblay and T. Gervais, Pixel-based open-space microfluidics for versatile surface processing, *Proc. Natl. Acad. Sci. U. S. A.*, 2021, **118**(2), 1–7, https://www.jstor.org/stable/27005899.
48 J. Autebert, *et al.*, Hierarchical hydrodynamic flow confinement: efficient use and retrieval of chemicals for microscale chemistry on surfaces, *Langmuir*, 2014, **30**(12), 3640–3645.
49 D. Huber, J. Autebert and G. V. Kaigala, Micro fluorescence in situ hybridization (μFISH) for spatially multiplexed analysis of a cell monolayer, *Biomed. Microdevices*, 2016, **18**(2), 40–40.
50 D. L. Andrews, G. D. Scholes and G. P. Wiederrecht, Comprehensive Nanoscience and Technology, *Nanomaterials*, 2011, **1**, 1–635.
51 L. X. Jiang, *et al.*, A monolithic microfluidic probe for ambient mass spectrometry imaging of biological tissues, *Lab Chip*, 2023, **23**(21), 4664–4673.
52 A. A. Kim, K. Kustanovich, D. Baratian, A. Ainla, M. Shaali, G. D. M. Jeffries and A. Jesorka, SU-8 free-standing microfluidic probes, *Biomicrofluidics*, 2017, **11**(1), 014112.
53 D. Qin, Y. Xia and G. M. Whitesides, Soft lithography for micro- and nanoscale patterning, *Nat. Protoc.*, 2010, **5**(3), 491–502.
54 M. Attaran, The rise of 3-D printing: The advantages of additive manufacturing over traditional manufacturing, *Bus. Horiz.*, 2017, **60**(5), 677–688.
55 ISO - ISO/ASTM 52900:2015 - Additive manufacturing — General principles — Terminology, 2021.
56 A. T. Brimmo, A. Menachery and M. A. Qasaimeh, Microelectrofluidic probe for sequential cell separation and patterning, *Lab Chip*, 2019, **19**(24), 4052–4063.
57 K. Takahashi, *et al.*, Stainless microfluidic probe with 2D-array microapertures, *AIP Adv.*, 2021, **11**(1), 015331.
58 X. T. Li, *et al.*, A Low-Cost, High-Resolution Thermoplastic Microfluidic Probe for Mass Spectrometry Imaging of Biological Tissue Samples, *Anal. Chem.*, 2025, **97**(6), 3207–3212.
59 X. F. van Kooten, J. Autebert and G. V. Kaigala, Passive removal of immiscible spacers from segmented flows in a microfluidic probe, *Appl. Phys. Lett.*, 2015, **106**(7), 074102.
60 P. Liu, *et al.*, Microfluidic Probe for In-Situ Extraction of Adherent Cancer Cells to Detect Heterogeneity Difference by Electrospray Ionization Mass Spectrometry, *Anal. Chem.*, 2020, **92**(11), 7900–7906.
61 X. T. Li, *et al.*, An Integrated Microfluidic Probe for Mass Spectrometry Imaging of Biological Samples, *Angew. Chem., Int. Ed.*, 2020, **59**(50), 22388–22391.
62 X. T. Li, H. Hu and J. Laskin, High-resolution integrated microfluidic probe for mass spectrometry imaging of biological tissues, *Anal. Chim. Acta*, 2023, **1279**, 341830, DOI: 10.1016/j.aca.2023.341830.
63 L. X. Jiang and J. Laskin, Pneumatically Assisted Microfluidic Probe for Enhanced Mass Spectrometry Imaging Performance, *J. Am. Soc. Mass Spectrom.*, 2025, **36**(4), 883–887.
64 S. Sofela, A. Saleh and M. A. Qasaimeh, *2022 International Conference on Manipulation, Automation and Robotics at Small Scales (MARSS)*, IEEE, 2022.
65 H. Luo, *et al.*, Region-specific control of lipid membrane fusion using an open-space fluidic online mixing system, *Sens. Actuators, B*, 2025, **430**, 137323, DOI: 10.1016/j.snb.2025.137323.
66 M. N. Gurcan, *et al.*, Histopathological image analysis: a review, *IEEE Rev. Biomed. Eng.*, 2009, **2**, 147–171.
67 M. S. Kim, *et al.*, Breast Cancer Diagnosis Using a Microfluidic Multiplexed Immunohistochemistry Platform, *PLoS One*, 2010, **5**(5), e10441, DOI: 10.1371/journal.pone.0010441.
68 Y. Huang, J. C. Williams and S. M. Johnson, Brain slice on a chip: opportunities and challenges of applying microfluidic technology to intact tissues, *Lab Chip*, 2012, **12**(12), 2103–2117.
69 L. F. Horowitz, *et al.*, Microfluidics for interrogating live intact tissues, *Microsyst. Nanoeng.*, 2020, **6**(1), 69.
70 J. F. Cors, *et al.*, A compact and versatile microfluidic probe for local processing of tissue sections and biological specimens, *Rev. Sci. Instrum.*, 2014, **85**(3), 034301.
71 A. Sarkar, *et al.*, Microfluidic probe for single-cell analysis in adherent tissue culture, *Nat. Commun.*, 2014, **5**(1), 3421.
72 S. F. Mao, *et al.*, Adhesion analysis of single circulating tumor cells on a base layer of endothelial cells using open microfluidics, *Chem. Sci.*, 2018, **9**(39), 7694–7699.
73 D. S. Ali, *et al.*, Microfluidic mixing probe: generating multiple concentration-varying flow dipoles, *Sci. Rep.*, 2025, **15**(1), 2252.
74 H. Shiku, *et al.*, A microfluidic dual capillary probe to collect messenger RNA from adherent cells and spheroids, *Anal. Biochem.*, 2009, **385**(1), 138–142.
75 M. Horayama, *et al.*, Spatial chemical stimulation control in microenvironment by microfluidic probe integrated device for cell-based assay, *PLoS One*, 2016, **11**(12), e0168158.
76 R. D. Lovchik, *et al.*, Micro-immunohistochemistry using a microfluidic probe, *Lab Chip*, 2012, **12**(6), 1040–1043.
77 R. D. Lovchik, D. Taylor and G. Kaigala, Rapid micro-immunohistochemistry, *Microsyst. Nanoeng.*, 2020, **6**(1), 94.
78 A. Kashyap, *et al.*, Quantitative microimmunohistochemistry for the grading of immunostains on tumour tissues, *Nat. Biomed. Eng.*, 2019, **3**(6), 478–490.
79 X. Li, *et al.*, High-throughput nano-DESI mass spectrometry imaging of biological tissues using an integrated microfluidic probe, *Anal. Chem.*, 2022, **94**(27), 9690–9696.
80 S. Feng, *et al.*, In-situ monitoring calcium signaling through tumor microtubes for single cell-cell communication via an open microfluidic probe, *Biosens. Bioelectron.*, 2022, **206**, 114137.

81 Q. Zhang, *et al.*, In situ stable generation of reactive intermediates by open microfluidic probe for subcellular free radical attack and membrane labeling, *Angew. Chem., Int. Ed.*, 2021, **60**(15), 8483–8487.
82 L. Zhou, *et al.*, In situ single-cell stimulation and real-time electrochemical detection of lactate response using a microfluidic probe, *Anal. Chem.*, 2021, **93**(24), 8680–8686.
83 Y. Song, *et al.*, Chemical Plasma Membrane Perforation Generated by a Microfluidic Probe for Single-Cell Intracellular Protein Delivery, *ACS Appl. Mater. Interfaces*, 2024, **16**(18), 22958–22965.
84 A. Bondarenko, *et al.*, Electrochemical push-pull probe: from scanning electrochemical microscopy to multimodal altering of cell microenvironment, *Anal. Chem.*, 2015, **87**(8), 4479–4486.
85 Y. Song, *et al.*, In Situ Time-Controllable Chemical Plasma Membrane Injury by Microfluidic Probe Reveals Self-Repair Ability of Single Cells, *Adv. Mater. Technol.*, 2023, **8**(24), 2301147, DOI: 10.1002/admt.202301147.
86 S. Mao, C. Sato, Y. Suzuki, J. Yang, H. Zeng, H. Nakajima, M. Yang, J.-M. Lin and K. Uchiyama, Microchemical Pen: An Open Microreactor for Region-Selective Surface Modification, *ChemPhysChem*, 2017, **18**(11), 1402–1406.
87 C. M. Perrault, *et al.*, Integrated microfluidic probe station, *Rev. Sci. Instrum.*, 2010, **81**(11), 115107, DOI: 10.1063/1.3497302.
88 N. Ostromohov, M. Bercovici and G. V. Kaigala, Delivery of minimally dispersed liquid interfaces for sequential surface chemistry, *Lab Chip*, 2016, **16**(16), 3015–3023.
89 J. Autebert, *et al.*, Convection-enhanced biopatterning with recirculation of hydrodynamically confined nanoliter volumes of reagents, *Anal. Chem.*, 2016, **88**(6), 3235–3242.
90 E. Delamarche, *et al.*, Biopatterning: The art of patterning biomolecules on surfaces, *Langmuir*, 2021, **37**(32), 9637–9651.
91 D. P. Taylor, *et al.*, Centimeter-Scale Surface Interactions Using Hydrodynamic Flow Confinements, *Langmuir*, 2016, **32**(41), 10537–10544.
92 K. Shinha, W. Nihei and H. Kimura, A Microfluidic Probe Integrated Device for Spatiotemporal 3D Chemical Stimulation in Cells, *Micromachines*, 2020, **11**(7), 691.
93 D. Widerker, F. Paratore, M. Bercovici and G. Kaigala, Biointegrated Fluidic Milling, *Adv. Mater. Technol.*, 2021, **6**, 2000843, DOI: 10.1002/admt.202000843.
94 H. F. Lin, *et al.*, Robust Long-Nanowire Fabrication by Clean-Phase-Assisted Micro Chemical Pen for Enhanced Bioassay Sensitivity, *Anal. Chem.*, 2024, **96**(36), 14339–14347.
95 H. F. Lin, N. Kasai, N. Xu, H. Nakajima, S. Kato, H. Zeng, L. Jin-Ming, S. Mao and K. Uchiyama, Localized hydrodynamic flow confinement assisted nanowire sensor for ultrasensitive protein detection, *Biosens. Bioelectron.*, 2022, **218**, 114788, DOI: 10.1016/j.bios.2022.114788.
96 Y. Nishitani, *et al.*, Regioselective fabrication of gold nanowires using open-space laminar flow for attomolar protein detection, *Chem. Commun.*, 2022, **58**(27), 4308–4311.
97 A. Glia and M. A. Qasaimeh, Lego-Like Microfluidic Probe for Concentration Gradient Discretization: A Path Toward Complete Modularization*, in *2024 International Conference on Manipulation, Automation and Robotics at Small Scales (MARSS)*, Delft, Netherlands, 2024, pp. 1–6, DOI: 10.1109/MARSS61851.2024.10612711.